SIMULATED AND EXPERIMENTAL SLIDING MODE CONTROL OF A HYDRAULIC POSITIONING SYSTEM

A Thesis

Presented to

The Graduate Faculty of The University of Akron

In Partial Fulfillment

of the Requirements for the Degree

Master of Science

Nahom Abebe Wondimu

May, 2006

SIMULATED AND EXPERIMENTAL SLIDING MODE CONTROL

OF A HYDRAULIC POSITIONING SYSTEM

Nahom Abebe Wondimu

Thesis

Approved:	Accepted:
_____	_____
Dr. Celal Batur Advisor	Dr. Celal Batur Department Chair
_____	_____
Dr. Malik Elbuluk Faculty Reader	Dr. George K. Haritos Dean of the College
_____	_____
Dr. Dane Quinn Faculty Reader	Dr. George R. Newkome Dean of the Graduate School
	_____
	Date

ABSTRACT

This thesis illustrates the application of a non-linear robust control to deal with friction variations in a hydraulic positioning system. The hydraulic system is modeled using analytical and experimental identification techniques considering both linear and nonlinear dynamics of the system. In the literature the friction is usually modeled as a function of velocity which has static, Coulomb and viscous friction components. However, there are several fascinating properties observed in systems with friction. This research is aimed at investigating the friction phenomenon and performing experiments on hydraulic positioning system to validate the identification of dynamic friction model (behavior in pre-sliding friction regime). The LuGre friction model which combines the pre-sliding behavior as well as the steady state characteristics is used to model and predict the friction for the controller design. A sliding mode controller is developed which has a feedback linearizing component plus additional terms that explicitly deal with system uncertainties due to friction and other unknowns. The sliding mode controller performed well during the experiments and simulations.

ACKNOWLEDGMENTS

I would like to express my gratitude first to Dr. Celal Batur, my advisor for his mentoring, guidance, and support throughout the research and writing of this thesis. His patience and advice have helped me to remain on the path during the course of my research. I appreciate the contribution of Parker Hannifin Corporation for providing the hydraulic system parts needed for the project implementation.

I respectfully thank Dr. Malik Elbuluk and Dr. Dane Quinn for their willingness to serve on my thesis committee and for their suggestions. Dr Paul C. Lam and Ms. Billi Faye Copeland have provided me their positive encouragement and assistance in the course of my studies.

Sincere appreciation is also given to Mrs. Stacy Meier, Ms. Paula Dunjen, Ms. Stephanie L. Emerson, Mr. Clifford G. Bailey and Mr. Stephen M. Gerbetz, for their assistance to my graduate study.

I would like to thank all my friends who helped me get through two years of graduate school with their warm and motivating atmosphere.

Last but not least, I would like to thank my parents, Ms. Genet Abera and Dr. Abebe Wondimu, my sister and friend, Mrs. Rakeb Abebe, for all the love and support they have given me over the years. They put in me confidence and a drive for pursuing my Masters.

TABLE OF CONTENTS

LIST OF TABLES

LIST OF FIGURES

CHAPTER I

INTRODUCTION

1.1 INTRODUCTION

Hydraulic systems are used in a wide variety of industrial applications. These systems provide high force, stiffness, and durability suitable for applications in mining, machining equipment, and remote manipulator operations in unstructured environments such as ground, sea, and space applications. Therefore, controlling of position or force outputs of hydraulic actuators should be of great interest in industrial fields to perform with improved precision and repeatability.

In hydraulic actuator movement of rod, piston, and hydraulic fluids are subjected to friction. Friction in mechanical systems is a nonlinear phenomenon which can cause control problems such as static errors, limit cycles and stick-slip.

More accurate friction models have been recently proposed in the literature [1-4], introducing two different motion regimes, sliding and pre-sliding, and overcoming the discontinuity of the classical model by introducing a relation between friction force and relative displacement in the pre-sliding regime.Friction models that have been used in literature range from being simple constant force that opposes motion to a seven parameter including various behavioral characteristics such as stiction, pre-sliding, a negative viscous slope, frictional memory, and hysteresis.

1.2 Objectives of This Thesis

The objective of this thesis is to develop a hydraulic system model, investigate the friction phenomenon, obtain and identify a friction model. The other sub-objective is to develop and implement a control law that can cope with model uncertainties. The performance of the controller is also assessed effectively by performing several simulations and experiments in real-time environment so that the motion of the piston can be monitored and controlled. The control algorithm is based on the sliding mode control philosophy.

1.3 Thesis Overview

In this thesis, we focus on identifying the friction phenomenon and the design of a sliding mode control in dealing with model uncertainty. The layout of this thesis is organized as follows. Chapter II presents detailed investigation of components used for the hydraulic system. Chapter III presents the analytical and experimental modeling of the hydraulic system and reports the results of this identification. A brief description of friction phenomenon is given in chapter IV. Chapter V presents experimental identification of the LuGre friction model parameters, and the obtained results. Sliding mode control for the hydraulic system is developed in chapter VI. Chapter VII presents performance of sliding mode control through simulation and experiment. Finally, chapter VIII formulates the summary and further work to be done.

CHAPTER II

DESCRIPTION OF THE HYDRULIC SYSTEM

2.1 Introduction

The hydraulic system as shown in figure 2.1 is mainly based on the direct–operated proportional DC valve, double acting hydraulic cylinder from Parker Hannifin and digital signal processor (DSP) from dSPACE. The flow of hydraulic fluid to the cylinder is controlled by a proportional DC valve which has revolutionized the drive technology of high response control with voice coil drive (VCD) technology. The operating pressure of 200 PSI is generated using a hydraulic pump for the actuation system. The position of the hydraulic cylinder along its stroke is measured using a linear variable differential transformer (LVDT) while pressure transducers are used to measure the pressure in each hydraulic cylinder chamber.

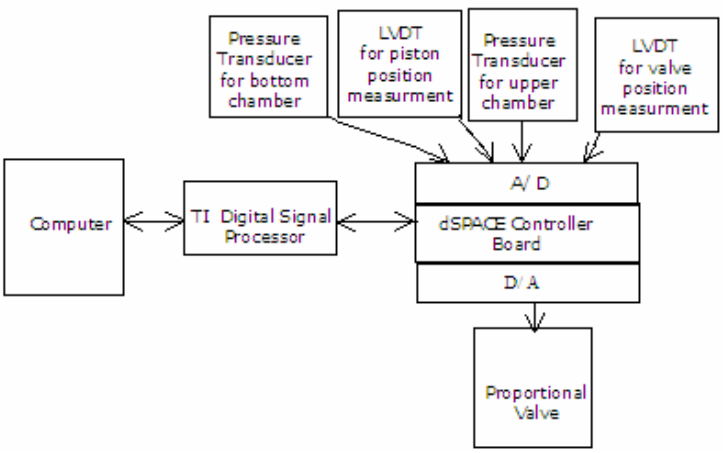

Figure 2.1 Electrical connection of the hydraulic system

Control and signal processing is done with a dSpace 1104 signal processor board, which includes onboard A/D and D/A converters and a slave digital signal processor (DSP). The schematic for electrical connection is shown in figure 2.1 and brief description of the hydraulic system is shown in figure 2.2.

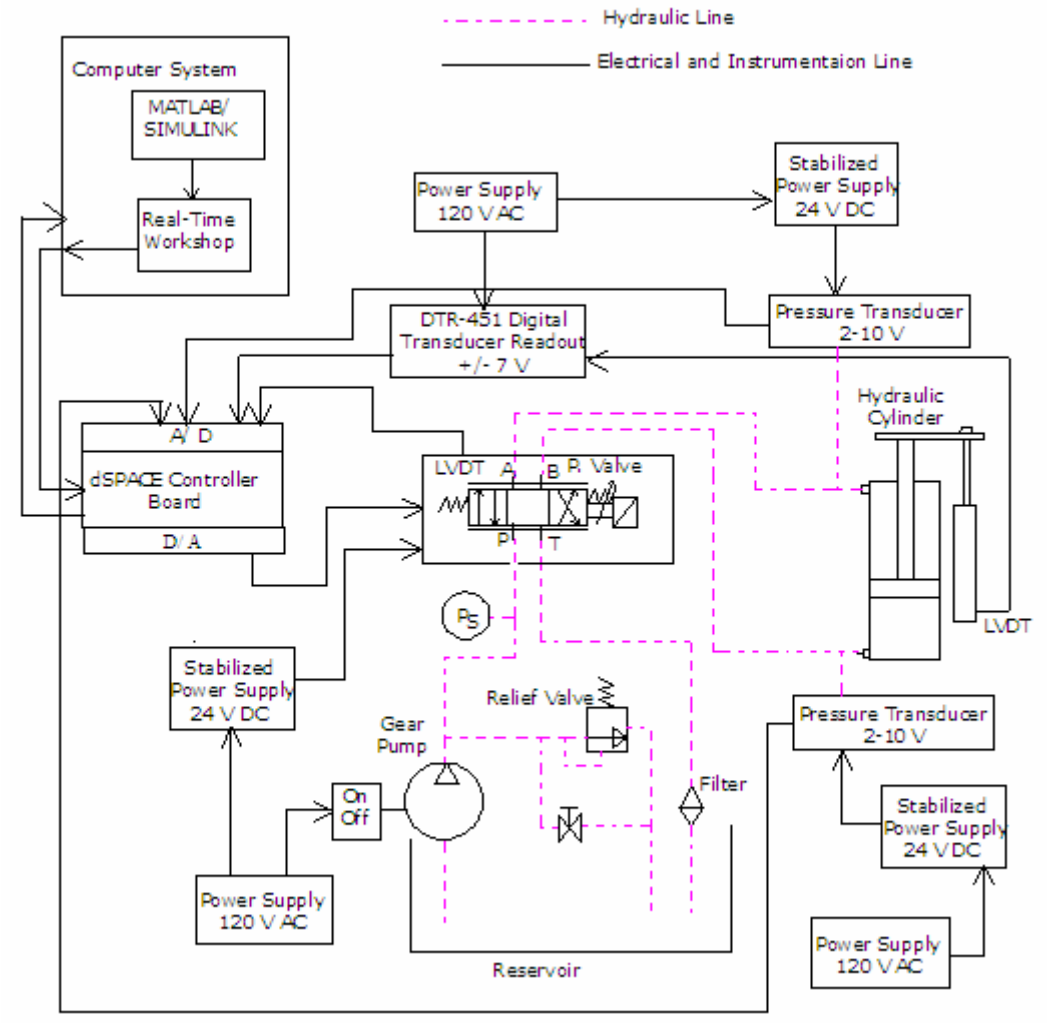

Figure 2.2 Process and instrumentation diagram of the hydraulic system

2.2 Hydraulic Cylinder (Model 1.5F3LLU519A6, Parker)

The cylinder shown in figure 2.3 has power stroke in both directions; hydraulic fluid is let in both directions for forward or return direction. It is set up in a vertical direction with no load except the weight of the piston and rod.

Table 2.1 Hydraulic cylinder physical parameters

Bore size	0.0381 m
Stroke length	0.1524 m
Piston rod diameter	0.015875m
Piston thickness	0.028575 m
Mass	0.5 Kg

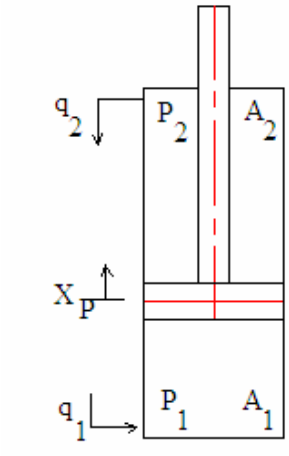

Figure 2.3 Schematic of a double acting actuator

2.3 Direct–Operated Proportional DC Valve (Model D1FPE01BC9NB5, Parker)

The direct–operated proportional DC valve shown in figure 2.4 is has revolutionized the drive technology of high response control with voice coil drive (VCD) technology.

In contrast to standard proportional solenoid drives, this technology actuates the spool using a movable coil. The spool is rigidly connected to the coil, which moves over a permanent magnetic cylinder free of friction. When the coil is energized, the spool is moved to the desired position. The valve is equipped with linear variable differential transformer (LVDT) to measure the spool position and the position signal is fed back into control electronics via a high resolution feedback system.

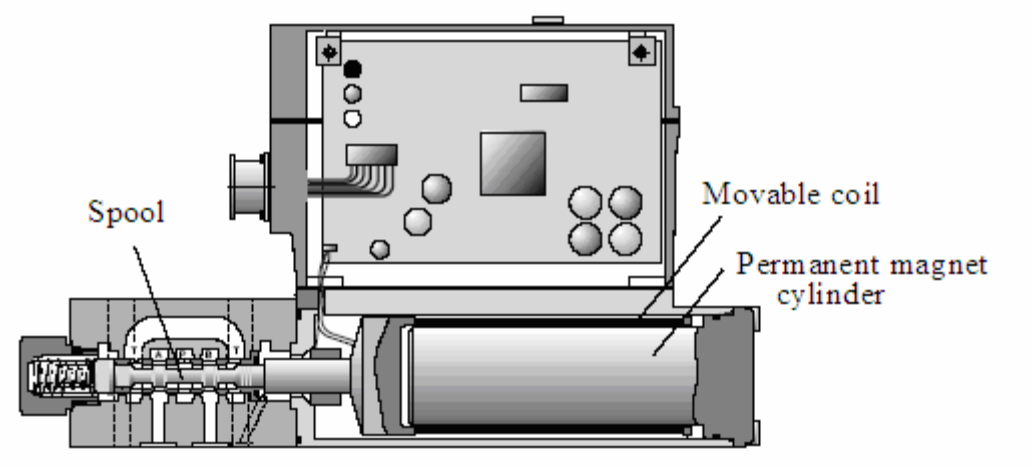

Figure 2.4 Direct-operated proportional DC valve (Courtesy of Parker Hannifin Corporation)

The direct-operated control valve D1FP features extremely high dynamics combined with maximum flow featuring bandwidth frequency of 300 Hz. The frequency response for the Parker DFplus valve with VCD shown in figure 2.5 is later used to compare with the experimentally determined frequency response of the valve.

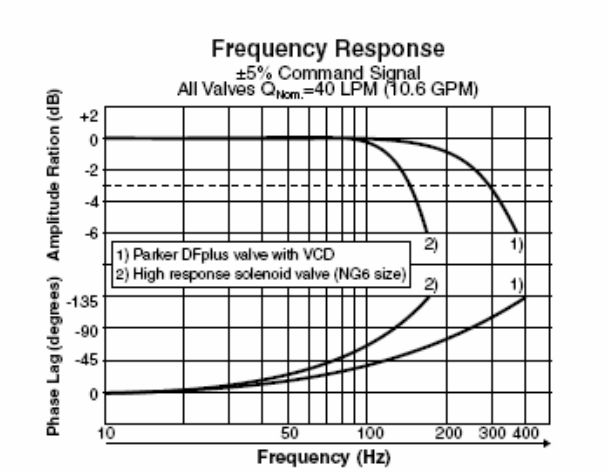

Figure 2.5 Frequency response of Direct-operated proportional DC valve (Courtesy of Parker Hannifin Corporation)

Table 2.2 Specifications of Direct-Operated Proportional DC valve (Courtesy of Parker Hannifin Corporation)

Actuation	Voice coil drive (VCD) actuator
Step response	<9ms at 100% step
Frequency response (± 5% signal)	300 (amplitude ratio -3dB) 250 (phase lag -90°)
Max operating pressure	Ports P, A, B 4500 PSI Port T 500 PSI
Flow (Nominal at ΔP=500 PSI per valve ports A and B	0.8 GPM
Flow maximum	21.2 GPM at ΔP=4500 PSI
Supply voltage	22V to 30V, ripple <5% eff.
Input signal	10V to -10V

2.4 Linear Variable-Differential Transformer (LVDT) and DTR-451 (Schaevitz)

LVDT is used to convert the linear displacement of the piston into an analog electrical signal. The Digital transducer readout (DTR) is a self contained, power line operated, high stability LVDT signal conditioner digital readout. It supplies a high frequency AC voltage for the LVDT and a -7 to 7 VDC analog output for A/D signal processor board.

2.5 Hydraulic Pump

A gear type hydraulic pump was used to supply constant pressure of to the hydraulic system.

Table 2.3 Hydraulic pump specifications

Motor	Baldor, CL3510
Voltage Input	120 AC
Operating Pressure	200 PSI G
Maximum Pressure	1000P PSI G

2.6 Pressure Transducers (Series PX215-300GI, Omega)

Pressure transducers are used to measure the pressure in each hydraulic cylinder chamber, where as the supply pressure is maintained at constant pressure of 200 PSI G. A simple circuit containing resistors is used to change the output current from transducers to voltage suitable for the A/D signal processor board.

Table 2.4 Specifications of Pressure transducers

Excitation	24Vdc
Output	4-20mA
Pressure rating	300PSI G

2.7 Digital Signal Processor Board (dSPACE 1104 Board)

Real-time control of the hydraulic system is implemented in MATLAB/SIMULINK and carried out using the Math Works Real-Time Workshop connected to dSPACE 1104 signal processor board around TMS320C31 floating point DSP which includes onboard A/D and D/A converters.

Table 2.3 Technical details of DS1102 controller board

Processor	TI's TMS320c31 floating-point DSP
Analog input	2 Parallel 16-bit channels, 4μs conversion time 2 Parallel 12-bit channels, 1.25μs conversion time ± 10 V input voltage range
Analog output	4 parallel 12-bit channels, 4μs settling time ± 10 V input voltage range
Digital I/O	Programmable digital-I/O subsystem based on TI's 25 MHz TMS320P14 DSP
	16 digital IO lines, PWM generation up to 6 channels
Physical Characteristics	+5 V, 1.5 A and ± 12 V, 100mA

Table 2.5 shows the maximum frequencies of the included timing applications for different channels in use, assuming that only one type of application is running at a time. The parameters of the controller implemented are changed and monitored through ControlDesk software. Figure 2.6 shows the interface developed in ControlDesk software later for controlling the hydraulic system.

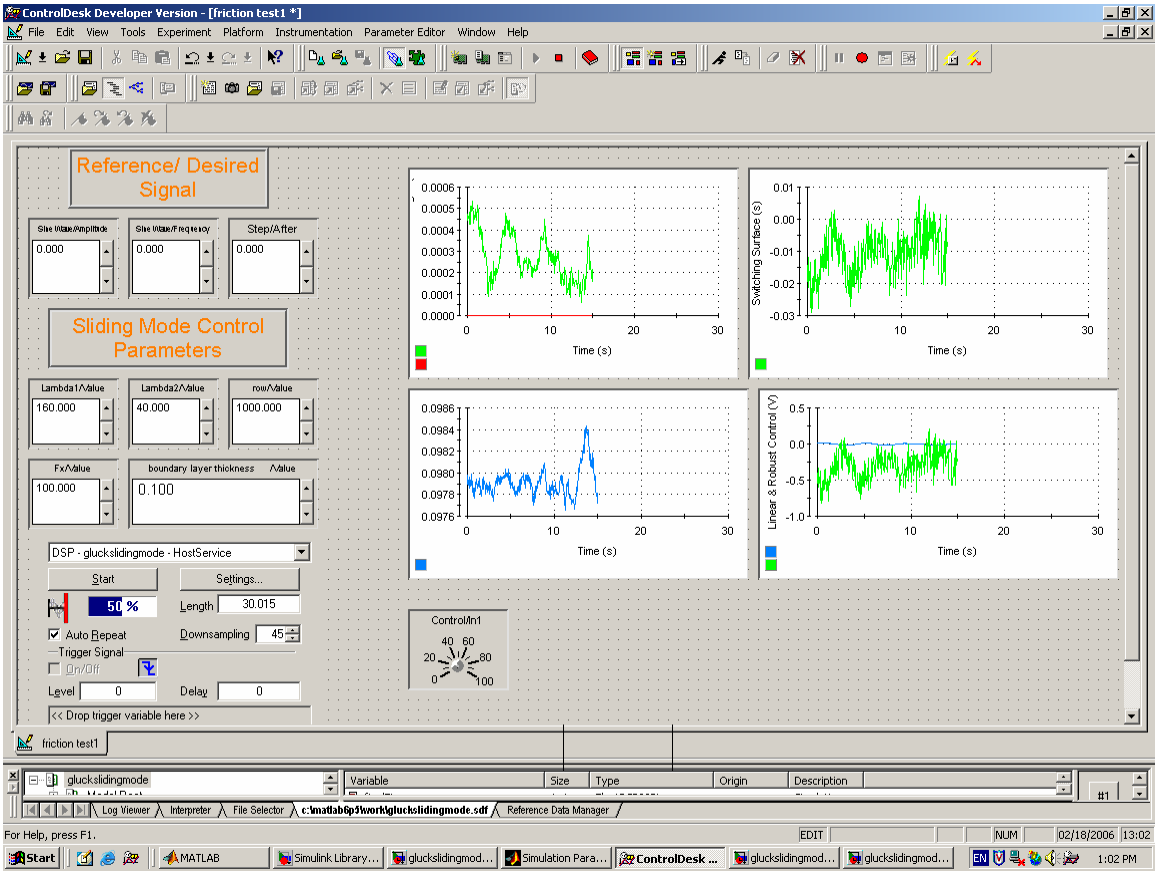

Figure 2.6 ControlDesk user interface developed for controlling position of the piston

2.8 Conclusions

This chapter gives detailed investigation on every components used for the hydraulic system. Study of all the measuring devices led to have accurate measurements as possible during experiments, and also the study of the different simulation and instrumentation software make it possible to fully utilize everything available.

CHAPTER III

THE HYDRAULIC SYSTEM MODEL

3.1 Introduction

The purpose of modeling the proportional valve and hydraulic actuator is to design a controller and predict or simulate the performance for the hydraulic system from the theoretical model obtained. Taking both linear and nonlinearities into account, a model for the hydraulic control system is derived and then nonlinear control is developed. The models will be validated through comparison of experimental and simulation results. The derivation of each the block shown in figure 3.1 will be briefly explained later.

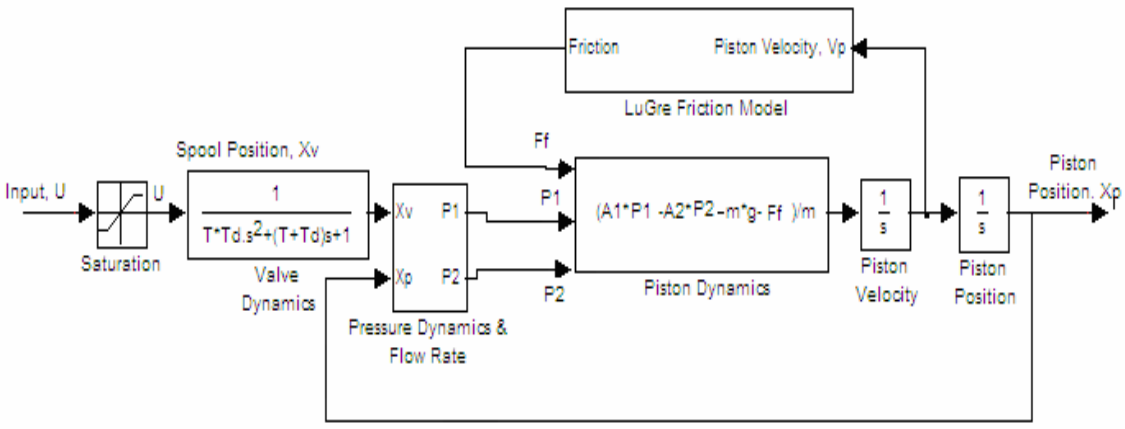

Figure 3.1 The open-loop block diagram for the hydraulic actuator system

3.2 System Identification by Frequency Response Method

Frequency response is a response of a system to sinusoidal inputs. The frequency response of a system consists of transfer functions that tell us how a system will respond to a sinusoidal input of any frequency. In the cases where we do not have a good model of the system and wish to determine the frequency response magnitude and phase experimentally, we can excite the system with sinusoidal signal by varying in frequency. The magnitude $G(s = j\omega)$ is obtained by measuring the ratio of the output sinusoid to the input sinusoid in the steady-state at each frequency. The phase angle $\angle G(j\omega)$ is the difference in phase between input and output signals.

A great deal can be learned about the dynamic response of a system from knowledge of the magnitude and phase of its transfer function. If the input signal is a sinusoid, then the magnitude and phase completely describe the response. Furthermore, if the input is periodic, then a Fourier series can be constructed to decompose the input into a sum of sinusoids, and again the magnitude and phase can be used with each component to construct the total response.

It is useful in control system design to indicate the bandwidth of the system. The bandwidth is a range the frequencies over which the system will be useful even if the system will not be driven with sinusoidal inputs. The value of the bandwidth assumed to be the frequency at which the magnitude of the frequency response ratio is -3 dB.

3.2.1 Direct-Operated Proportional DC Valve

Obtaining the model of the valve dynamics analytically is quite a bit of work and complicated but instead we obtained it by means of experimental analysis. The frequency response method is used to determine the transfer function. The amplitude ratio and phase shift of the spool output to input sinusoid signal have been measured at a sufficient number of frequencies with the frequency range of interest. It's then plotted in the Bode diagram, which is a plot of the logarithmic of the magnitude ratio and phase against the frequency on a logarithmic scale. Then the transfer function is determined by asymptotic approximations [8].

The transfer function to the input to valve, u(t) and output from valve, x_v(t) of the system is given by

$$G_{valve}(s) = \frac{X_V(s)}{U(s)} \tag{3.1}$$

To perform a frequency-response test, a sinusoidal-signal generated from the MATLAB software send to the proportional valve via the dSPACE board. Frequency ranges starting from 0.05 Hz to 410 Hz are used to excite the system using 5% command signal (amplitude of 0.5 V).

The values of amplitude ratio and phase shift for the frequency ranges obtained from experiment are shown in table A.1.

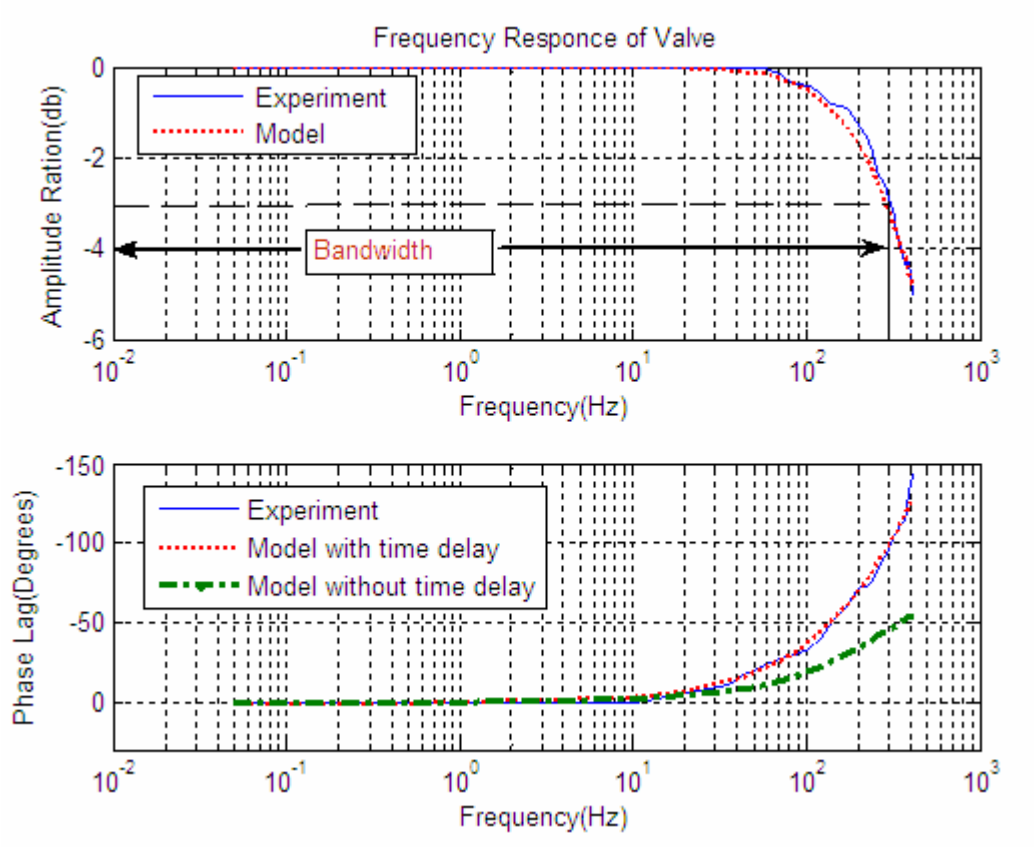

Figure 3.2 Frequency response of the proportional valve and approximation models

As shown in figure 3.2 the amplitude ratio and phase shift are plotted in a Bode diagram and the associated transfer function is determined from it. The frequency response is approximated by having a transfer function without time delay and is given by the transfer function

$$G_{valve}(s) = \frac{1}{\tau s + 1} \tag{3.2}$$

and better approximated by having a transfer function having a time delay of 0.5 msec given by

$$G_{valve}(s) = \frac{1}{\tau s + 1} e^{-\tau_d s} \tag{3.3}$$

where τ is the time constant, and τ_d is the time delay. Approximation of the delay time, τ_d is done using Taylor's series expansion of first order derivative about (s = 0) is given by

$$f(s) = f(0) + \dot{f}(0)(s) \quad , \quad \text{where } f(s) = e^{-\tau_d s} \tag{3.4}$$

$$e^{-\tau_d s} = 1 - \tau_d s \cong \frac{1}{\tau_d s + 1} \tag{3.5}$$

Therefore equation (3.3) can be written as

$$G_{valve}(s) = \frac{1}{\tau\tau_d s^2 + (\tau + \tau_d)s + 1} \tag{3.6}$$

The frequency response obtained from the test resembles the manufacturer's frequency response (5% command signal) diagram which is shown in figure 2.4. It is also confirmed here again that it has a bandwidth of 300 Hz, time constant of 0.00056 sec and time delay of 0.0005 sec.

3.2.2 Hydraulic Cylinder

The non-linear model of the hydraulic cylinder is done analytically later, but here assuming as a linear model, the transfer function of the cylinder is obtained from the frequency response method. The values of amplitude ratio and phase shift of the piston position to the spool position for certain frequency ranges obtained from experiment are shown in table A.2.

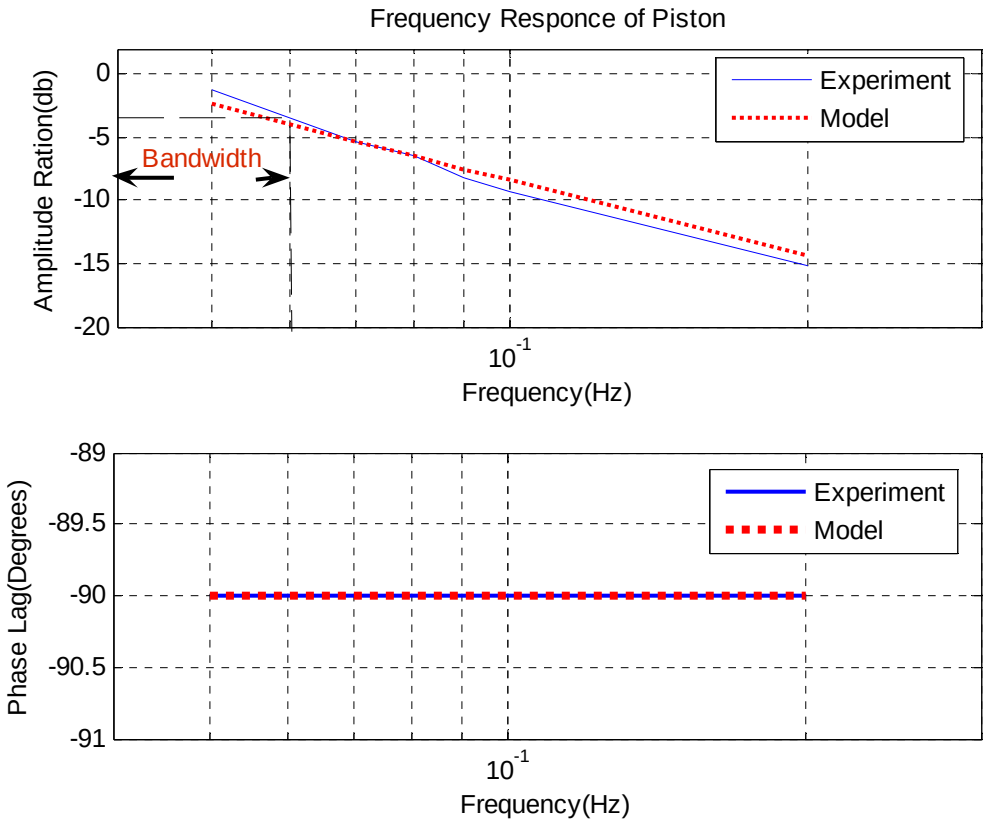

Figure 3.3 Frequency response of the hydraulic piston

The transfer function associated to figure 3.3 is found to be

$$G_{piston}(s) = \frac{X_P(s)}{X_V(s)} \tag{3.7}$$

$$G_{piston}(s) = \frac{K}{s} \tag{3.8}$$

Where the gain, K is the intersection of frequency asymptote to the 0-dB line and is found to be 0.2. The bandwidth is of the hydraulic piston is observed to be close to 0.06 Hz.

3.3 System Identification by Step and Pulse Response Method

The steady state behavior of the piston for the step and pulse input can also be used to determine the transfer function of the system. This test is performed to validate the linear model obtained previously between the piston and the valve.

3.3.1 Step Response

The transfer function between the valve and the piston position can be found by observing the response of the steady state velocity of the piston. The step output from the valve to the piston is given by the equation:

$$u(t) = 0, \quad \text{for } t < 0 \qquad (3.9)$$

$$= A, \quad \text{for } t > 0$$

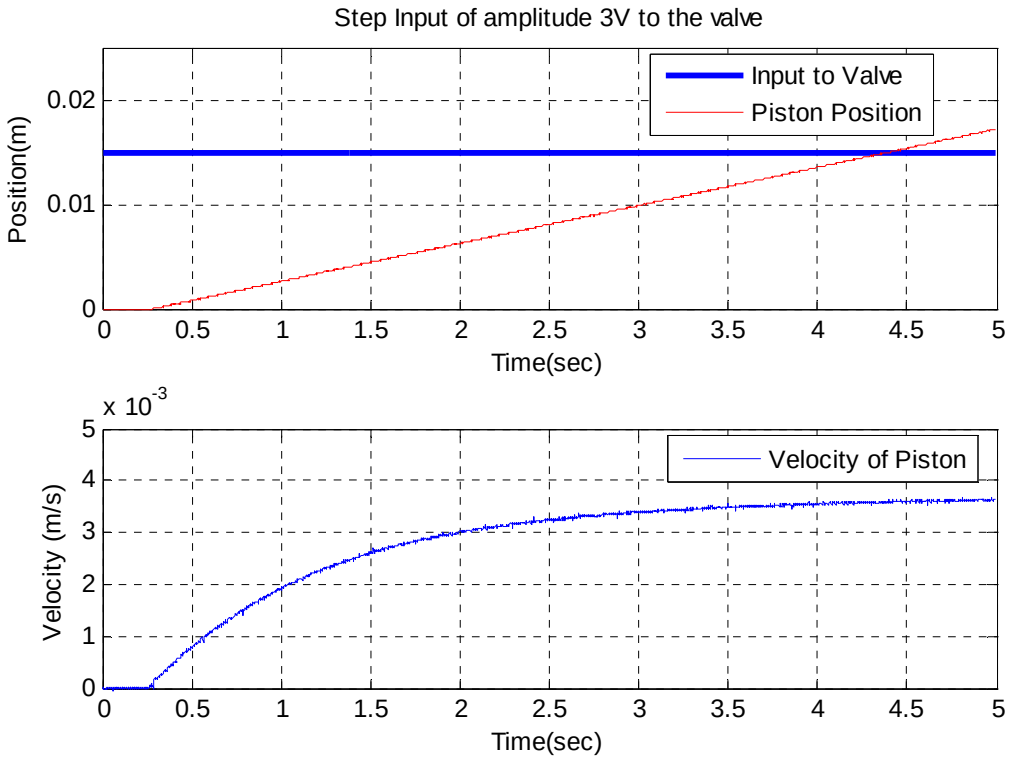

Figure 3.4 Response of the piston to a step output from the valve

The valve line in figure 3.4 indicates time change in step input where as the amplitude is arbitrary. The velocity of the piston is obtained by taking derivative of the position signal and passing it through a low pass filter to reduce the noise.

The open loop transfer function of the system can be given by combining equation (3.5) and equation (3.7)

$$G_{system}(s) = G_{piston}(s) \; . \; G_{valve}(s) \tag{3.10}$$

$$\frac{X_P(s)}{U(s)} = \frac{K}{s(\tau\tau_d s^2 + (\tau + \tau_d)s + 1)} \tag{3.11}$$

We can write the above equation to represent the velocity of piston under the condition that u(t) is a step input of amplitude A:

$$\dot{X}_P(s) = \frac{K}{(\tau\tau_d s^2 + (\tau + \tau_d)s + 1)} \frac{A}{s} \tag{3.12}$$

Using final value theorem [8] the steady state behavior of $\dot{x}_P(t)$ as t approaches infinity is be given by

$$\dot{x}_P(\infty) = K\ A \tag{3.13}$$

From figure 3.3, the steady state velocity of piston can be approximated and as a result the value K is determined to be 0.236.

3.3.2 Pulse Response

The transfer function between the valve and the piston position is also found by observing the response of the steady state position of the piston to a pulse input to the valve is given by

$$u(t) = A, \quad \text{for } 0 < t < t_0 \qquad (3.14)$$

$$= 0, \quad \text{for } t < 0,\ t_0 < t$$

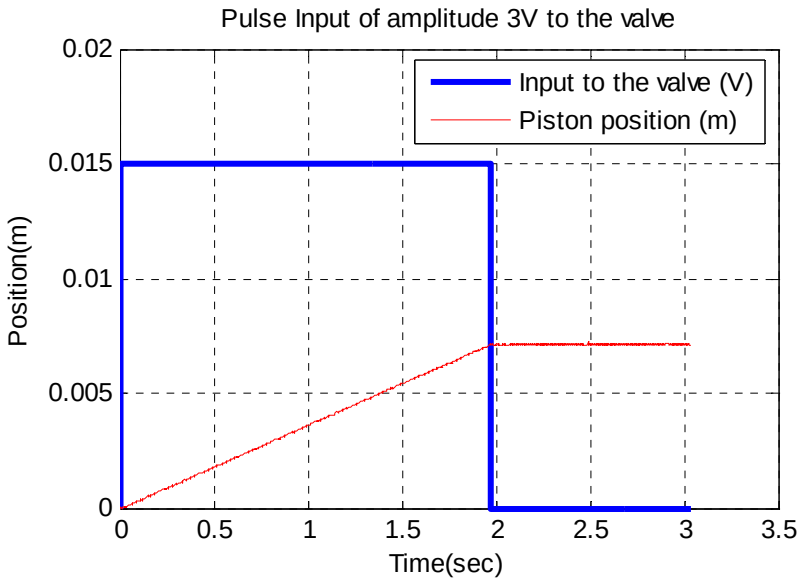

Figure 3.5 Response of piston to a pulse output from the valve

The valve line in figure 3.4 indicates time change in pulse input where as the amplitude is arbitrary. The velocity of the piston is obtained by taking derivative of the position signal and passing it through a low pass filter to reduce the noise. Writing equation (3.9) to represent the position of the piston for the pulse input we obtain:

$$X_P(s) = \frac{K}{s(\tau\tau_d s^2 + (\tau + \tau_d)s + 1)}\left(\frac{A}{s} - \frac{A}{s}e^{-t_0 s}\right) \qquad (3.15)$$

Using the final value theorem [8] the steady state behavior of $x_P(t)$ as t approaches infinity is be given by

$$x_P(\infty) = \text{K A } t_0 \tag{3.16}$$

Using figure 3.4, the steady state position can be approximated and as a result the value K is determined to be 0.24.

3.4 Flow Rate Through Proportional Valve

The position of the proportional valve spool controls the flow rate in, q_1 and out, q_2 of the hydraulic actuator. However the flow rate also depends on the supply pressure, P_S, the tank pressure, P_T, and the pressure in the bottom actuator chamber, P_1, and the upper chamber, P_2.

The turbulent flows through the control orifices of the valve, to and from the two sides of the cylinder chambers, are modeled by nonlinear expressions[3,6]. Assuming positive flow directions as shown in figure 2.2, we have

$$q_1 = C_v x_v (sgn(x_v) \sqrt{(P_s - P_1)} + \text{sgn}(-x_v)\sqrt{(P_1 - P_R)}), \tag{3.17}$$

$$q_2 = C_v x_v (sgn(x_v) \sqrt{(P_s - P_2)} + \text{sgn}(-x_v)\sqrt{(P_2 - P_T)}), \tag{3.18}$$

Where C_v is the proportional valve coefficient for all the valve ports and $\text{sgn}(x_v)$ is a sign function that indicates the spool is extending or retracting and is given by

$$sgn(x_v) = 1, \qquad x_v \geq 0 \tag{3.19}$$

$$= 0, \qquad x_v < 0$$

Starting with the continuity equation and taking the fluid compressibility into account, it can be shown that the pressure dynamics [3, 6] are given by

$$\frac{dP_1}{dt} = \frac{\beta}{V_1}(-\dot{V}_1 + q_1 - q_{leakage}) \tag{3.20}$$

$$\frac{dP_2}{dt} = \frac{\beta}{V_2}(-\dot{V}_2 - q_2 - q_{leakage})$$

(3.21)

Where V_1 and V_2

$$V_1 = V_{01} + A_1 x_p \tag{3.22}$$

$$V_2 = V_{02} - A_2 x_p \tag{3.23}$$

Where A_1 and A_2 represent the effective areas of the bottom and the top face of the piston respectively. V_{01} and V_{02} are the volumes of the bottom and top chamber of the cylinder, respectively corresponding to position ($x_p = 0$) of the piston. The fluid bulk modulus is denoted by β, and the leakage flow, $q_{leakage}$ is assumed to be negligible.

3.5 Valve Parameter and Fluid Bulk Modulus Identification

The proportional valve coefficient, C_v and the fluid bulk modulus, β have to be determined to calculate the flow rates across the valve. The least squares analysis of the data obtained from several open loop tests was used to identify the parameters [17]. In order to use the least squares analysis, we first need an equation in the form of ($XA = Y$).

According to equation (3.17) the flow equations for the hydraulic valve by taking the tank pressure equal to zero and for positive direction of the valve motion can be given as:

$$q_1 = C_v x_v \sqrt{P_S - P_1} \tag{3.24}$$

$\dot{P}_1$ from equation (3.20) for negligible leakage flows, $q_{leakage}$ can written as follows

$$\dot{P}_1 = \frac{\beta}{V_1}(-\dot{V}_1 + q_1) \tag{3.25}$$

Incorporating V_1 into (3.25) through (3.22)

$$\dot{P}_1(V_0 + A_1 x_P) = \beta(-A_1 \dot{x}_P + q_1) \tag{3.26}$$

Substituting equation (3.24) in terms of q_1 in (3.26), we can derive the equation

$$\frac{-1}{\beta}\dot{P}_1(V_0 + A_1 x_P) + C_v x_v \sqrt{P_s - P_1} = A_1 \dot{x}_P \tag{3.27}$$

Which can be written XA=Y form

$$\begin{bmatrix} \dot{P}_{1,i}(T_i)V_0 + A_1 \dot{x}_{P,i}(T_i) & x_{v,i}(T_i)\sqrt{P_s(T_i) - P_{1,i}(T_i)} \end{bmatrix} \begin{bmatrix} \frac{-1}{\beta} \\ C_v \end{bmatrix} = \begin{bmatrix} A_1 \dot{x}_{P,i}(T_i) \end{bmatrix} \tag{3.28}$$

Where i= 1, 2,…, N

Now the above equation is in the form ($XA = Y$) where x_v, x_p, P_1 and P_2 are sampled data from experiment using the sampling period of T. The derivatives ($\dot{P}_1, \dot{P}_2$ and $\dot{x}_p$) are obtained through numerical differentiation. We can approximate $\hat{A}$ which will give the sum of least square error and can be calculated as

$$\hat{A} = \begin{bmatrix} 1/\hat{\beta} \\ \hat{C}_v \end{bmatrix} = (X^T X)^{-1} Y \tag{3.29}$$

As shown in the figure 3.6, a sinusoidal input is applied to the valve and only the part of the data when the valve moves in the positive direction is used in (3.29).

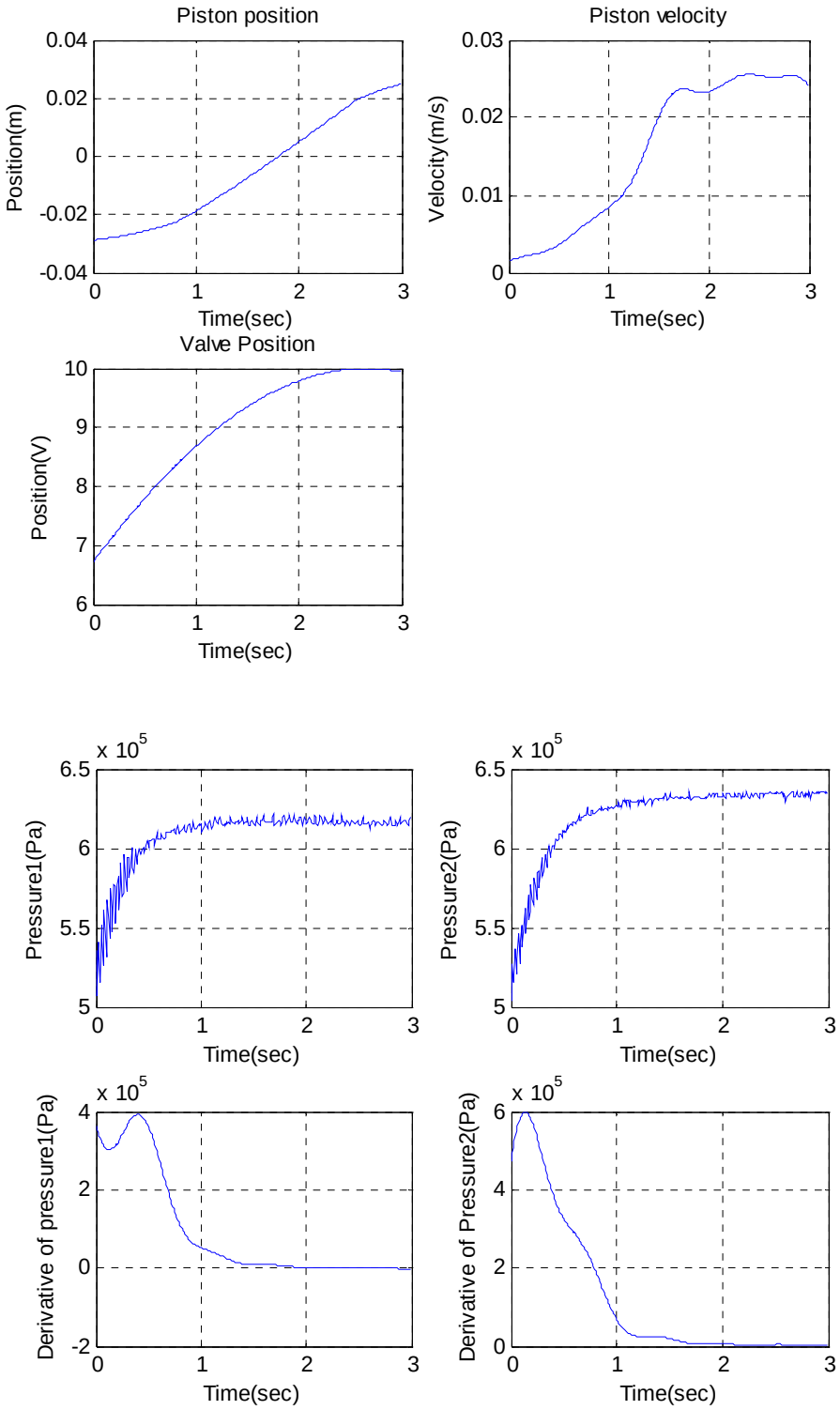

Figure 3.6 Data obtained from experiment for a positive direction of the valve for a sinusoidal wave input

A least squares analysis of the data obtained from several sinusoidal open loop tests experiments for the valve parameter and bulk modulus are averaged to get good estimates ($\beta = 1.816 \times 10^6 \frac{N}{m^2}$ and $C_v = 2.863 \times 10^{-9} \frac{m^2}{s.V.\sqrt{Pa}}$).

3.6 Hydraulic Piston Dynamics

Applying Newton's second law to a hydraulic piston yields the equation of motion for an actuator given by

$$\ddot{x}_P = \frac{1}{m}(P_1 A_1 - P_2 A_2 - mg - F_f) \tag{3.30}$$

Where $\ddot{x}_P$ is the acceleration of the piston, m is the mass of piston and rod, F_f is the friction opposing the axial motion, and g is the gravitational acceleration of the earth. The non-linear friction force which includes stiction, Coulomb, Stribeck, and viscous components is discussed in next chapters.

3.7 Conclusions

This chapter presents the analytical and experimental modeling of the hydraulic system. A second-order model is derived between the spool position of the proportional valve and the input voltage applied from the computer. System identification methods by frequency, step and pulse response methods are used to determine the transfer function between the valve and the piston has shown the same result. Analytical models for the flow rate through the valve and pressure dynamics are also done. At this point we have developed transfer functions for the valve and the piston based on experimental Bode

plots. We have also developed a non-linear model for the proportional valve and the hydraulic actuator. The linear model for the valve is used to make comparison with the company data. The same will later be used in the controller design. The nonlinear dynamic model of the cylinder will be used later in Chapter VII when we design the sliding mode controller.

CHAPTER IV

FRICTION IN HYDRAULIC ACTUATORS

4.1 Introduction

Friction is a nonlinear phenomenon which occurs in all mechanical equipments such as hydraulic systems, and leads to deterioration of performance. It is therefore important for engineers to study and understand the friction phenomenon acting on different systems.

Friction is usually modeled as a function of velocity which has static, Coulomb and viscous friction components. However, there are several fascinating properties observed in systems with friction. In applications with high precision positioning and with low velocity tracking a better description of the friction phenomenon is necessary.

Detailed analysis of friction experiments shows that there are two friction regions: pre-sliding and sliding regions. In the pre-sliding region the friction force is considered to be a function of the bristle deflections (figure 4.3) as the force at the bristle contacts are dominant.

Armstrong-Helouvry *et al*. [3] drive a general model structure which includes several experimentally observed friction properties. Many of the information in this chapter came from the review of friction research by C. Canudas de Wit, P. Noel, A. Aubin, and B. Brogliato [1], C. Canudas de Wit, H. Olsson, K.J. Astrom, and P. Lischinksy [2, 5].

4.2 Static Models of Fiction

The static models describe friction as a force which opposes motion and its magnitude is only dependent on velocity. It is also described by a discontinuous relation between the friction force and the relative velocity.

Leonardo Da Vinci (1519) proposed the first classic model of friction which assumes that the friction force is proportional to the normal load and the net deriving force on an object is the difference between the applied force and the friction force [15].

Coulomb (1785) further developed the Da Vinci's friction model and the friction phenomena described by the model known as Coulomb friction [15].

$$F_f = F_c \, sgn(\dot{x}) \tag{4.1}$$

Where

$$sgn(\dot{x}) = 1, \qquad \dot{x} \geq 0 \tag{4.2}$$

$$= 0, \qquad \dot{x} < 0$$

and the friction force, F_c is proportional to the normal load given by

$$F_c = \mu_D \, F_N, \tag{4.3}$$

Where μ_D describes the dynamic coefficient of friction force, F_N is the normal force, and $\dot{x}$ is the velocity of the moving object.

Morin (1833) stated the basic model of friction, that there is a maximum force named static force, F_s which has to be overcome before any movement occurs[15]

$$F_s = \mu_s \, F_N \tag{4.4}$$

Where μ_s is the static coefficient of friction and it is always greater than the dynamic coefficient friction, μ_D.

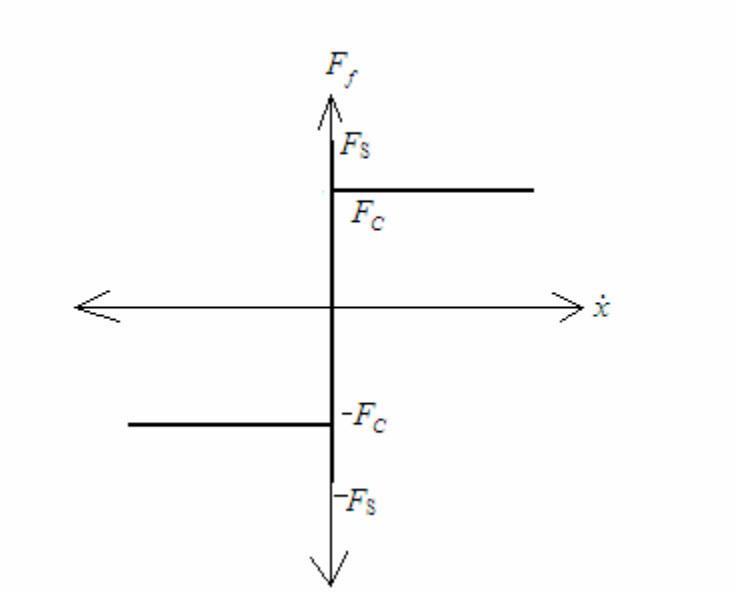

Figure 4.1 Static plus Coulomb friction model

Reynolds (1866) developed expressions for the friction force caused by the viscosity of lubricants [5]. The viscous friction is described as

$$F_v = \mu_v \dot{x} \tag{4.5}$$

Where μ_v is the viscous damping coefficient, $\dot{x}$ is the velocity of the moving object. Then the friction model becomes:

$$\begin{aligned} F_f &= F_{s,} && |\dot{x}| = 0 \\ &= F_c + F_v, && |\dot{x}| > 0 \end{aligned} \tag{4.6}$$

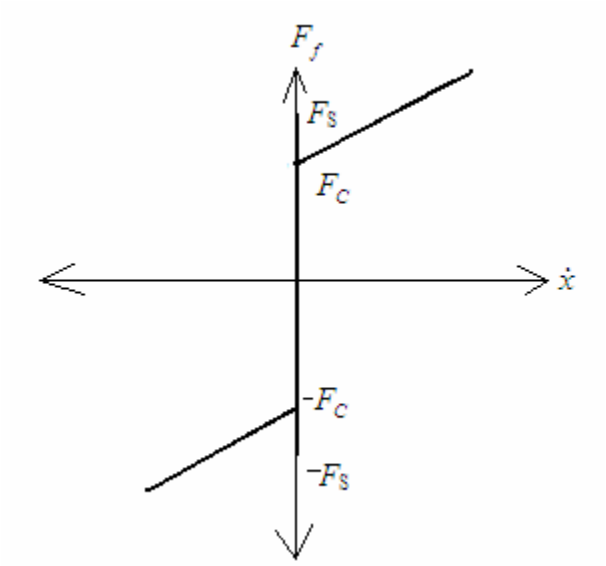

Figure 4.2 The static, Coulomb, viscous friction model (Classical model)

4.3 Dynamic Models of Friction

One of the main problems with the classical model is the discontinuity between static friction and dynamic friction regimes. The classical model uses a switching function between the two regimes. Such a switching function is physically not justified and may result in implementation problems.

Stribeck (1902) observed that for low velocities, the friction force is decreasing continuously with increasing velocities[15]. This phenomenon of a decreasing friction at low, increasing velocities is called the Stribeck friction or effect. The change in friction from dynamic (pre-sliding region) to static (sliding region) is recognized as being continuous as shown in figure 4.4.

4.3.1 The Dahl Model

Dahl [11] developed a friction model for the purpose of simulating control systems with friction. The model was comparatively a simple model which was used extensively to simulate systems with ball bearing friction and which has been also used as a standard simulation model in the aerospace industry. Dahl observed that surfaces are very irregular at the microscopic level and two surfaces make contact at a number of asperities, which can be thought of as elastic bristles in combination with lubricant effects. As shown in figure 4.3, Dahl modeled the bristle as elastic springs.

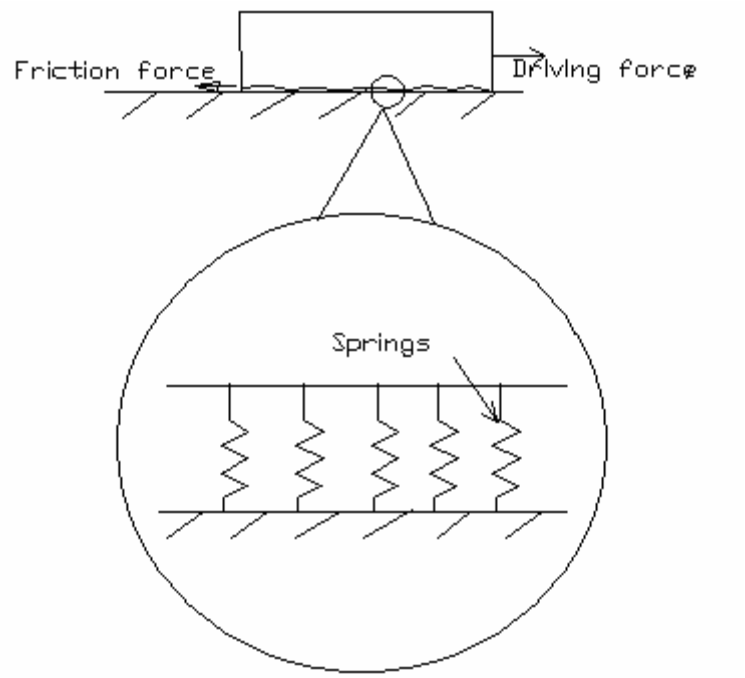

Figure 4.3 Dahl's spring model

Dahl used the theory from the stress-strain curve in classical solid mechanics [12]. He interpreted friction as the friction force increases gradually until rupture occurs when

subjected to stress. The friction model is seen to behave as a nonlinear 'soft' spring with a nearly linear elastic curve for small deflections. Dahl modeled the friction force using

$$\frac{dF_f}{dx} = \sigma(1 - \frac{F_f}{F_C}\text{sgn}(\dot{x}))^{\alpha} \tag{4.7}$$

Where F_c is the coulomb friction which can also be interpreted as a yield force σ is the stiffness coefficient and α is the parameter that determines the shape of the stress-strain curve. In this model friction force is only a function of the displacement and the sign of the velocity. This implies that friction force is only position dependent. To obtain a time domain model Dahl observed that

$$\frac{dF_f}{dt} = \frac{dF_f}{dx}\frac{dx}{dt} \tag{4.8}$$

Therefore, equation 4.7 can be written as

$$\frac{dF_f}{dt} = \sigma(1 - \frac{F_f}{F_C}\text{sgn}(\dot{x}))^{\alpha}\,\dot{x} \tag{4.9}$$

Introducing F = σ z, the model can be written as

$$\frac{dz}{dt} = \dot{x} - \frac{\sigma\,|\,\dot{x}\,|}{F_c}z \tag{4.10}$$

4.3.2 The Bristle and Reset Integrator Model

Haessig and Friedland introduced a friction model in [4], which attempted to design the irregularities in the contact surfaces or the bristles as springs giving rise to friction. The contact between the surfaces thought as a bond between flexible bristles. The bond

strain assumed to increase as the surfaces move relative to each other and increasing the friction force. The fiction force is given by

$$F_f = \sum_{i=1}^{N} \sigma_0 (x_i - b_i) \tag{4.11}$$

Where N is the number of bristles, σ_0 the stiffness of the bristles, x_i the relative position of the bristles, and b_i is the location where the bond was formed. As $| x_i - b_i |$ equals δ_s the bond is assumed to break and a new one is formed at a random location. The model captures fascinating properties of friction but motion in sticking may be oscillatory since there is no damping of the bristles in the model and it is inefficient in simulations.

Haessig and Friedland also proposed the reset integrator model as an alternative to the bristle model. They assume that breakage does not occur but the bond is kept constant after it reaches the point of rapture. The friction force is given by

$$F_f = (1+a\,(z))\ \sigma_0\,(\dot{x})\,z + \sigma_1 \frac{dz}{dt} \tag{4.12}$$

$$\frac{dz}{dt} = 0, \quad \text{if } (\dot{x} > 0 \text{ and } z \geq z_0) \text{ or } (\dot{x} < 0 \text{ and } z \leq -z_0) \tag{4.13}$$

$$= \dot{x}, \quad \text{otherwise}$$

$$a(z) = \text{a}, \quad \text{if } |z| < z_0 \tag{4.14}$$

$$= 0, \text{ otherwise}$$

Where $\sigma_1 \frac{dz}{dt}$ is the damping term, and *a(z)* is a function which determines the bristle deflection. As the deflection reaches its maximum value z_0, the variable z remains constant. The reset integrator model is efficient to simulate but it is necessary to detect when $|z| \geq z_0$.

4.3.3 The LuGre Model

A model which has combined the Dahl's [11] consideration and employing the idea of averaged deformation of bristles [4] has been developed at the universities of Lund and Grenoble [2] and is called the LuGre friction model. When a tangential force is applied to two surfaces, the bristles will deflect like springs, and if the deflection is sufficiently large the bristles start to slip.

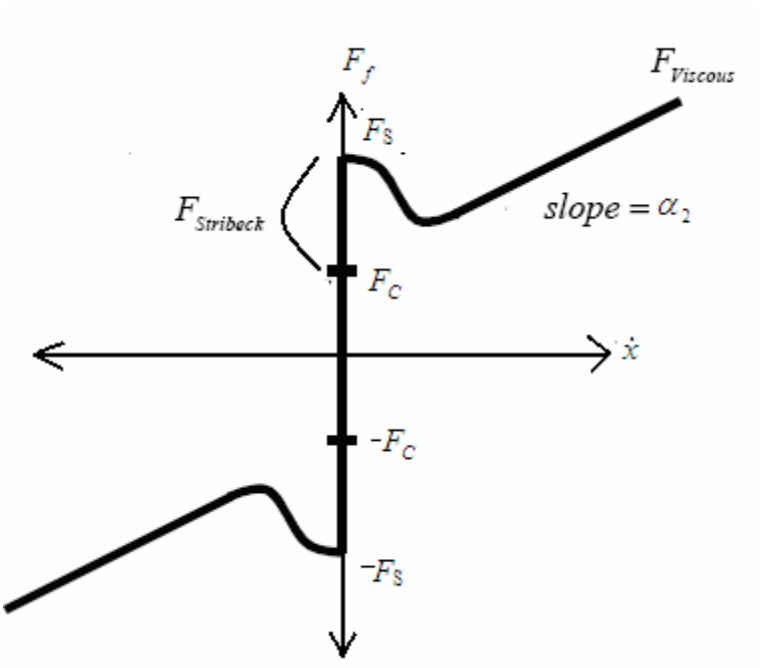

Figure 4.4 The static, Coulomb, viscous plus Stribeck friction model (Dynamic model)

The LuGre friction model which combines the pre-sliding behavior of the Dahl model with the steady state friction characteristics like Coulomb friction, viscous friction and the Stribeck effect is shown in figure 4.4. The LuGre friction model uses an internal state variable z (bristle deflection) governed by

$$\frac{dz}{dt} = \dot{x} - \sigma_0 \frac{|\dot{x}|}{g(\dot{x})} z \tag{4.15}$$

Where $\dot{x}$ is the relative velocity between the two surfaces, and σ_0 is the bristle stiffness parameter. The Stribeck function, $g(\dot{x})$ is a decreasing function for increasing velocity bounded by upper limit equal to Stiction (static friction) force and a lower limit equals to the Coulomb friction force, and v_s the Stribeck velocity:

$$g(\dot{x}) = \alpha_0 + \alpha_1 e^{-(\frac{\dot{x}}{v_s})^2} \tag{4.16}$$

The corresponding friction force is described by

$$F_f = \sigma_0 z + \sigma_1 \frac{dz}{dt} + \alpha_2 \dot{x} \tag{4.17}$$

Where $\frac{dz}{dt}$ the average bristle deflection, and α_2 is the viscous friction coefficient. In equation (4.17) the first two terms denote the force generated by bristle interactions and the last term is the viscous friction force.

4.3.4 The Leuven Model

The Leuven model, presented by the authors [18] was based on the experimental findings that the friction force in pre-sliding regime is a hysteresis function of the position, with non-local memory, which was only approximated by the former models. The Leuven model tries to fit this specific behavior into the LuGre-model in order to obtain better tracking.

4.4 Conclusions

This chapter briefly discusses the progress and the development of friction from static to dynamic models. In applications with high precision positioning and with low

velocity tracking a better description of the friction phenomenon using the dynamic model is necessary because of the low velocities and especially crossing of the zero velocity. LuGre friction model is chosen for predicting the friction for the hydraulic system since it captures most of the behavior friction. In the next chapters the LuGre friction model approach will be used to model the friction in the hydraulic actuator, and also to predict the friction of the piston for the sliding mode control.

CHAPTER V

IDENTIFICATION OF FRICTION PARAMETERS

5.1 Introduction

Most of the static and dynamic characteristics of the friction in the LuGre friction model appear as a non-linear and are tough to estimate. It is thus important to investigate identification mechanisms to estimate the different parameters and derive the friction model. The identification of the friction parameters is divided into static (parameters affecting the sliding region) and dynamic (parameters affecting the pre-sliding region) of the friction.

Various ways of identifying the friction parameters have been reviewed from literature [9,14]. We have performed many experiments to have good estimates of the friction parameters, and also validation of the friction model has been done by comparing simulation and experiment for open and closed loop response of the piston.

5.2 Static Friction Parameters Identification

The static parameters of the LuGre friction model are responsible for the behavior of the friction in the sliding region. The static parameters for the LuGre friction model are the coulomb friction, α_0, the Stribeck friction, α_1, the viscous friction, α_2, and the Stribeck velocity, v_s as stated in chapter 4 .

5.2.1 Stiction Force

The stiction force or sometimes called static friction force is the sum of the Coulomb friction, α_0 and the Stribeck friction, α_1 from the LuGre friction model.

The equation of motion for the hydraulic actuator (3.30) can be written to calculate for friction as

$$F_f = P_1 A_1 - P_2 A_2 - mg - m\ddot{x}_P \tag{5.1}$$

The driving force to the piston is calculated from the pressure measurements at on each side of the piston, and is given by

$$F_{driving} = P_1 A_1 - P_2 A_2 \tag{5.2}$$

where P_1 is the pressure in the bottom actuator chamber, and P_2 is the pressure in the upper actuator chamber . The driving force, $F_{driving}$ can be understood as the sum of the friction force acting on the piston and weight of the piston before the piston starts to move. The maximum value of the driving force can be assumed to be the sum of the stiction (static friction) force and the weight of the piston. Therefore combining equation (5.1) and (5.2) for zero acceleration (no motion of piston) gives

$$F_{driving} = F_f + mg \tag{5.3}$$

The static friction has been estimated by applying a very slow ramp input in an open loop and taking the value of the driving force at the time instant when the hydraulic piston motion starts. An experimental test is conducted by measuring the pressure at both ports of the cylinder and the piston position while applying a very slow ramp input to the valve.

The driving force is calculated from the pressure data, and also the velocity of the piston is obtained by taking derivative of the position signal and passing it through a low pass filter ($\frac{1}{0.4s+1}$) to reduce the noise in the velocity data. The valve line in figure 5.1 and figure 5.2 indicates time change in the ramp input where as the amplitude is arbitrary.

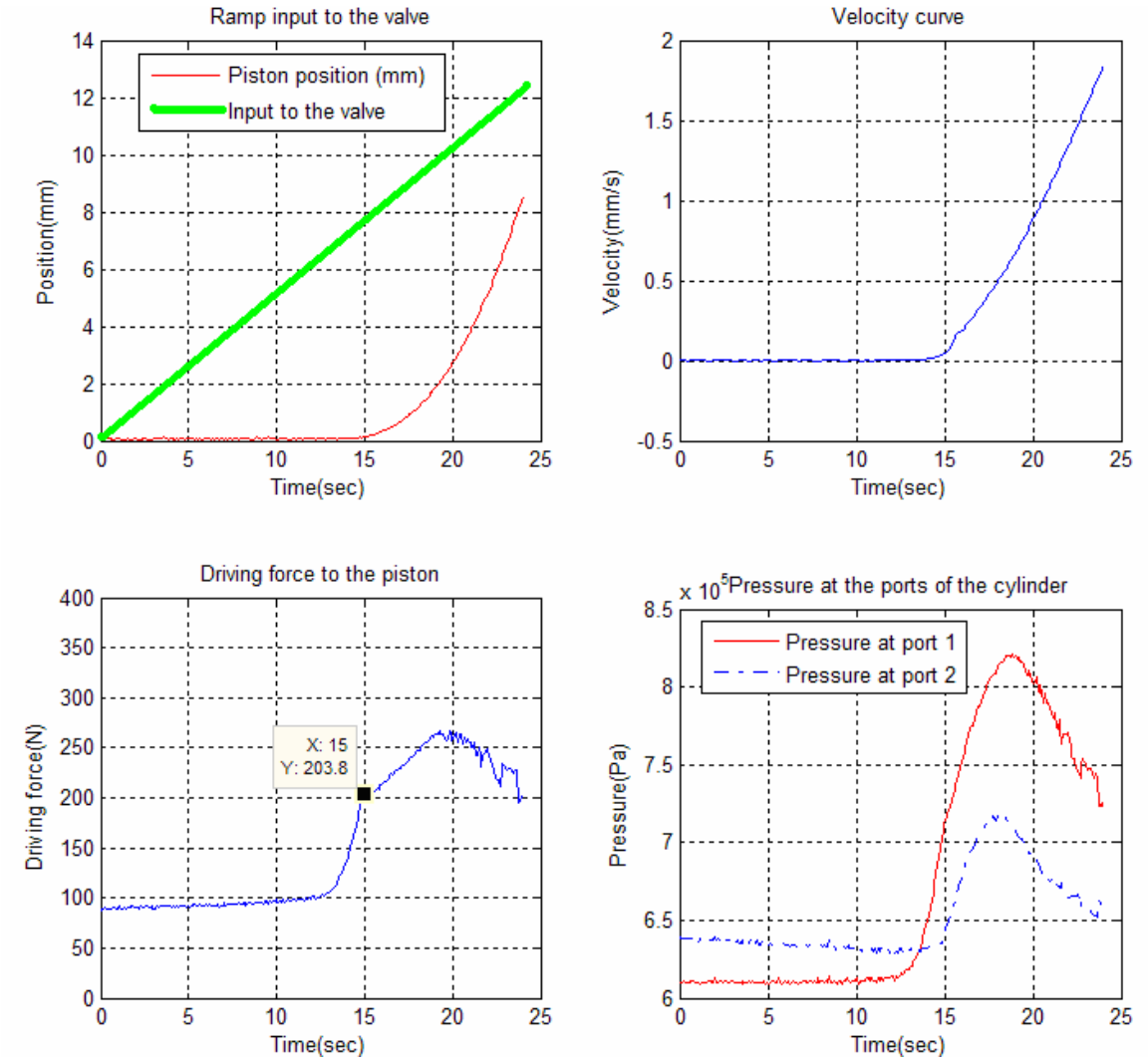

Figure 5.1 Stiction force estimation for zero initial position of the piston (xp(0)= 0 mm)

As it can be seen from the above figure 5.1 for zero initial position of the piston the value of the driving force at the instant the piston starts to move is found to be 203.8 N, and static friction is calculated to be 198.9 N since the weight of the piston 4.9 N.

These kinds of experiments have been done for different initial positions of the piston ranging from the bottom to the top cylinder end. Figure 5.2 shows data obtained for different initial positions of the piston.

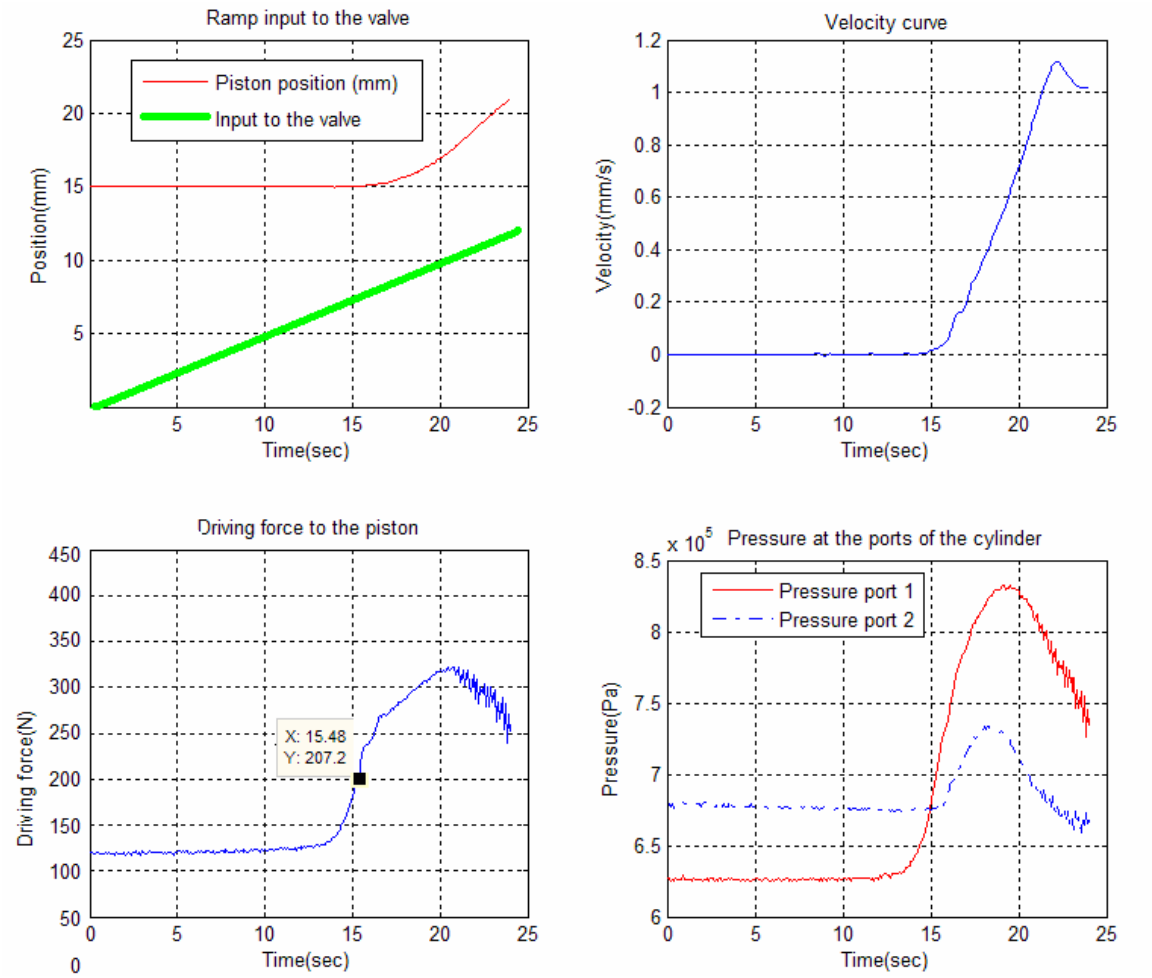

Figure 5.2 Stiction friction estimation for initial position (xp(0) = 15 mm)

From figure 5.2 the static friction force is calculated to be 202.3 N different from the previously obtained result of 198.9 N. These kinds of variations in stiction force have

been also observed from in other experiments performed for different initial positions of the piston.

The unevenly distributed stiction along the cylinder also motivated us to see the repeatability of the friction. Again another set of experiments have been done at the same initial positions and obtained different results of stiction. All values of stiction force obtained for the different cases stated previously are summarized in figure 5.3.

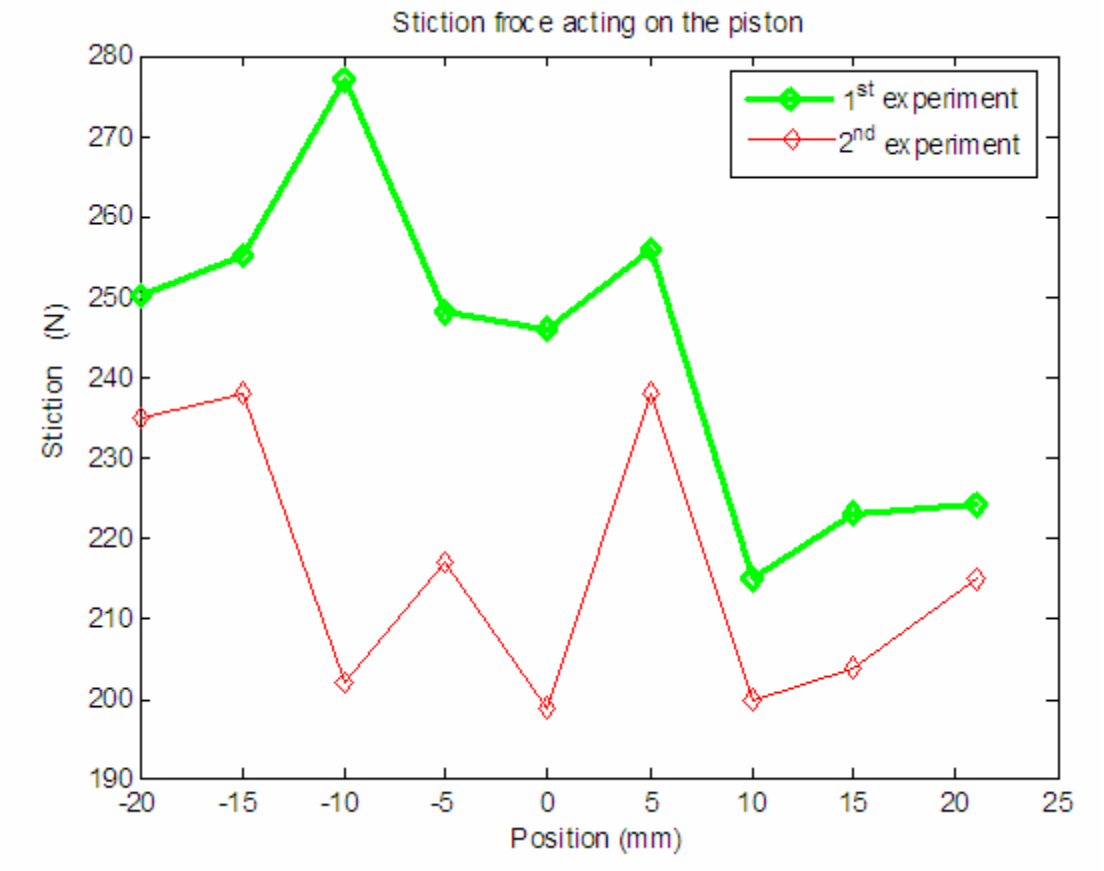

Figure 5.3 Stiction force acting on the piston at different initial positions of the piston

The 1st and 2nd experiments from figure 5.3 corresponds to performing tests just after running the hydraulic system, and after 45 minutes of running the hydraulic system respectively . We can see that the value of stiction force acting on the piston is dependent on the initial position and time. The dependency of stiction force on time can be interpreted as a change in temperature since the hydraulic fluid, and also the piston and the wall of the cylinder temperature increases after running the hydraulic system for long time. The value of the stiction force obtained from the experiment is averaged to 240 N. However, we avoided taking the value of the averaged stiction force value for granted but just used it as initial guess for the numerical curve fitting which was performed later.

5.2.2 Coulomb, Viscous Coefficient and Stribeck Velocity Friction Parameter

The Coulomb and viscous coefficient friction parameters are estimated by construction of the friction velocity map measured during constant velocity motions. From the knowledge of the step response of the piston (chapter III) it is possible to obtain (after transient) a constant velocity of the piston by applying a step input to the valve. We know that, the steady state velocities lead to zero acceleration. Therefore, the friction for steady state velocities or zero acceleration can be given by

$$F_f = P_1 A_1 - P_2 A_2 - mg \tag{5.4}$$

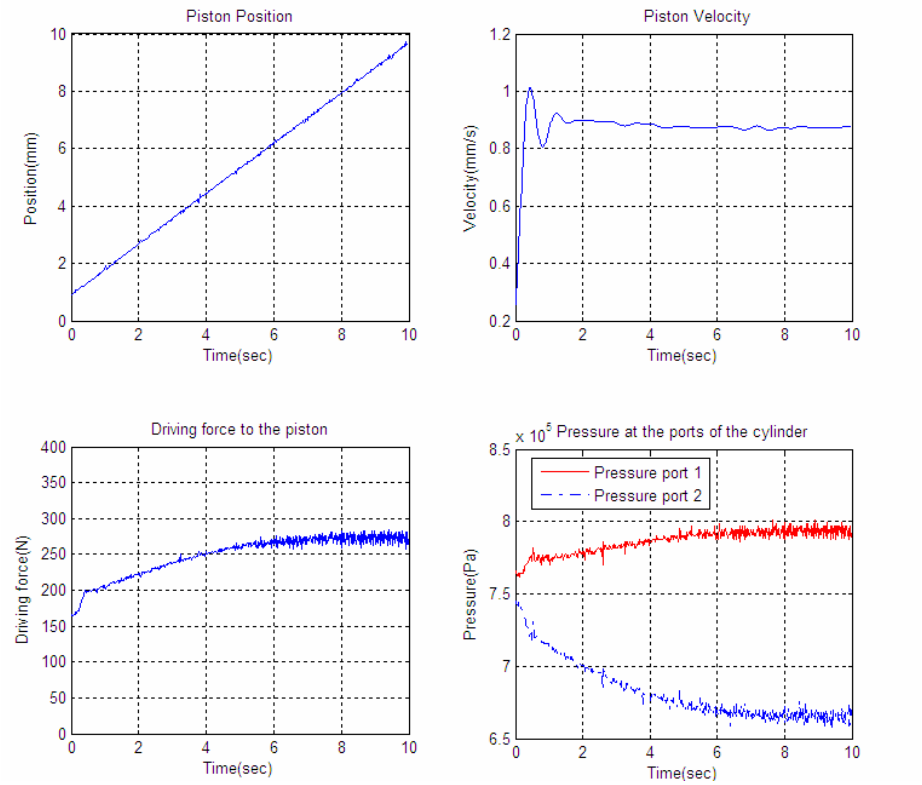

Figure 5.4 Friction estimation at constant velocity of the piston

One of the several experiments performed for steady state velocities ranging from 0.04 mm/s to 41mm/s is shown in figure 5.4. A large number of steady state friction points are also collected at low velocity in order to improve identification of the Stribeck velocity.

The model used for friction is the LuGre model as discussed in chapter IV, repeated here for convenience

$$\frac{dz}{dt} = \dot{x}_p - \sigma_0 \frac{|\dot{x}_p|}{g(\dot{x}_p)} z \tag{5.5}$$

$$g(\dot{x}_p) = \alpha_0 + \alpha_1 e^{-(\frac{\dot{x}_p}{v_s})^2}$$

(5.6)

$$F_f = \sigma_0 z + \sigma_1 \frac{dz}{dt} + \alpha_2 \dot{x}_p \tag{5.7}$$

At steady state friction (friction at constant velocity), we can assume rate of deflection, $\frac{dz}{dt}$ equals to zero, because once the piston start moving the bristles slip away after elongating to their maximum length (average bristle deflection, z will be constant). After the piston motion starts, equation (5.5) becomes

$$0 = \dot{x}_p - \sigma_0 \frac{|\dot{x}_p|}{g(\dot{x}_p)} z \quad \text{or} \tag{5.8}$$

$$z = \frac{\dot{x}_p}{|\dot{x}_p|} \frac{g(\dot{x}_p)}{\sigma_0} \tag{5.9}$$

We can simplify equation (5.9) knowing, $sgn(\dot{x}_p) = \frac{\dot{x}_p}{|\dot{x}_p|}$

$$z = \frac{g(\dot{x}_p)}{\sigma_0} sgn(\dot{x}_p) \tag{5.10}$$

The friction can be estimated by substituting equation (5.10) into (5.7) :

$$\hat{F}_f = \hat{g}(\dot{x}_p)\, sgn(\dot{x}_p) + \hat{\alpha}_2 \dot{x}_p \tag{5.11}$$

Substituting equation (5.6) into (5.11) in terms of the Stribeck function gives

$$\hat{F}_f = (\hat{\alpha}_0 + \hat{\alpha}_1 e^{-(\frac{\dot{x}_p}{\hat{v}_s})^2})\, sgn(\dot{x}_p) + \hat{\alpha}_2 \dot{x}_p \tag{5.12}$$

The friction values, F_f obtained from steady state velocities of the piston is plotted in friction- velocity map as shown in figure 5.5.

Nonlinear least squares optimization algorithm [13] from MATLAB is used to fit the experimental data shown in figure 5.5 into equation (5.12). The experimental data is used to search for $\hat{\alpha}_0$, $\hat{\alpha}_1$, $\hat{v}_s$ and $\hat{\alpha}_2$ that minimizes the output error function :

$$E\left\{(F_f, \hat{F}_f); \hat{\alpha}_0, \hat{\alpha}_1, \hat{v}_s, \hat{\alpha}_2\right\} = \sum_{i=1}^{n} [F_f(\dot{x}_{pi}) - \hat{F}_f(\dot{x}_{pi})]^2 \qquad (5.13)$$

where $F_f(\dot{x}_{pi})$ are the experimentally obtained friction values measured at constant velocities of the piston, and $\hat{F}_f(\dot{x}_{pi})$ is given by equation (5.12) . A good curve fit to the experimental data is obtained as it is shown in figure 5.5.

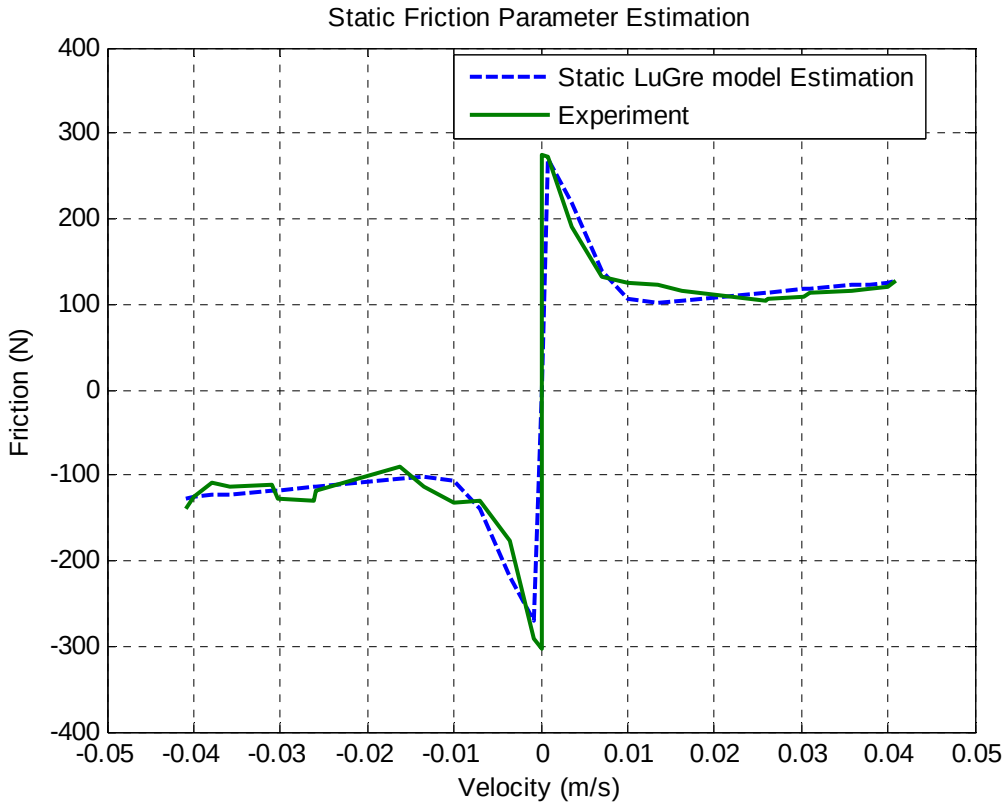

Figure 5.5 Static friction-velocity map experimental and estimation

The estimated values of the static friction parameters are summarized in table 5.1

Table 5.1 Static LuGre friction parameters

Static Friction Parameters		Estimated values
Stiction	$\alpha_0 + \alpha_1$	273 N
Coulomb friction	α_0	89 N
Stribeck friction	α_1	184 N
Viscous coefficient	α_2	920 N.s/m
Stribeck velocity	v_s	5.8×10^{-3} m/s

5.3 Dynamic Friction Parameter Identification

The dynamic parameters σ_0 and σ_1 are much more difficult to determine because the average bristles deflection, *z* is not measurable. A good estimation of the dynamic friction parameters can be made using the non-linear optimization methods. However, for a successful estimation of the dynamic parameters a reasonable initial guess is necessary.

During the open loop motion of the piston for very slowly changing ramp input to the valve, $\dot{x}_p$ and $\frac{dz}{dt}$ can be assumed negligible for very low velocities. Therefore equation (5.6) and (5.7) become

$$g(\dot{x}_p) = \alpha_0 + \alpha_1 \tag{5.14}$$

$$F_f = \sigma_0 z \tag{5.15}$$

Substituting (5.14) and (5.15) into (5.5) gives,

$$\frac{dz}{dt} = \dot{x}_p - \frac{|\dot{x}_p|}{\alpha_0 + \alpha_1} F_f \tag{5.16}$$

Where the friction force for zero acceleration is approximated by

$$F_f = P_1 A_1 - P_2 A_2 - mg \tag{5.17}$$

The average bristles deflection is computed from the numerical integration of (5.16) to obtain $z(t)$ where the friction and velocity are obtained from experiment. The numerical integration is performed using MATLAB/ SIMULINK software by representing the equations as a block diagram as shown in figure B.1. The initial guess for $\hat{\sigma}_0$ is calculated from the friction data obtained from equation (5.17) and the value z obtained from numerical integration of (5.16). Therefore, the value of $\hat{\sigma}_0$ can be calculated by averaging the data from (5.15) as:

$$\hat{\sigma}_0 \approx \frac{z^T F_f}{z^T z} \tag{5.17}$$

Where z is a vector found by integrating (5.17) and F_f is also a vector obtained from (5.17) by taking sampled data from experiment (P_1, P_2 and $\dot{x}_P$). Now precise value of the dynamic parameters is calculated by using SIMULINK to simulate the open loop system model given by equation (5.1), (5.5), (5.6) and (5.7) while changing the dynamic parameters to get the same response of the piston position as the experiment.

The block diagram representation using equation (5.5), (5.6) and (5.7) is shown in figure 5.6 which shows that the friction can be calculated from the piston velocity measurement. Now we can simulate the open loop system model using (5.1) and also by

using the flow rate and pressure dynamics equation given in the previous chapters.

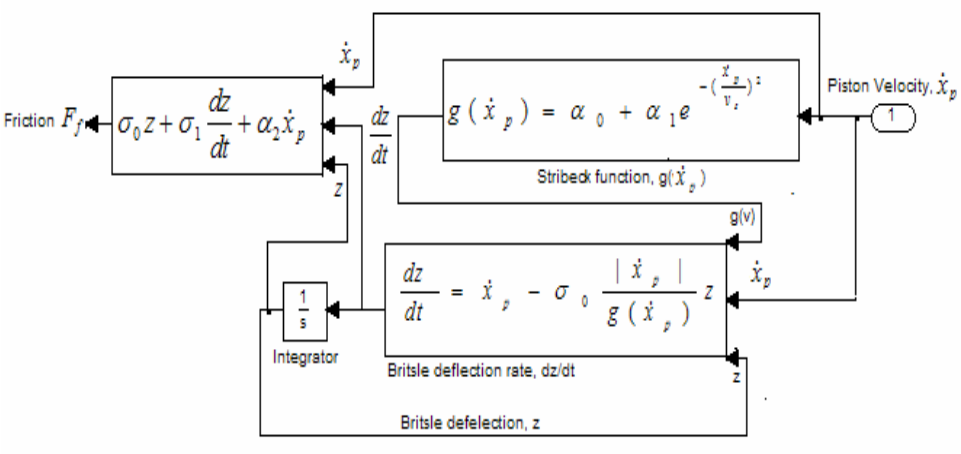

Figure 5.6 Block diagram representation of the LuGre friction model

Experiments are performed as shown in figure 5.7 using a slowly changing ramp input to the valve. The advantage of the slowly changing ramp input is to capture the friction force before it gets to the stiction force as well as to obtain the Stribeck part of the fiction which occurs at low velocities.

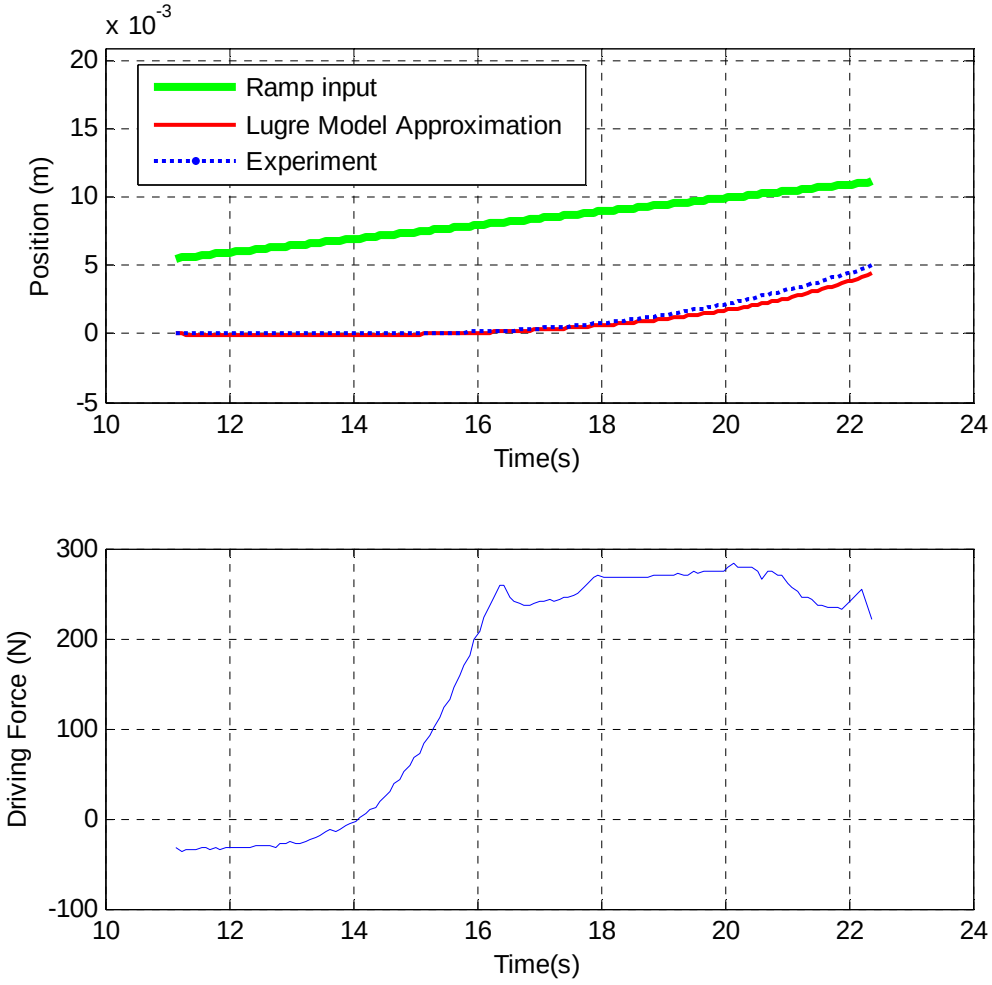

Figure 5.7 Friction estimation using the open loop response of the piston for the initial position of (xp(0)= 0 m)

The pre-sliding region from figure 5.7 can be described as the region before the piston motion starts while increasing the driving force. A good approximation to the experimental response is achieved by changing the values of the dynamic parameters of the LuGre friction model as shown in figure 5.7 and figure 5.8. Again another set of experiments have been done at different initial positions of the piston and we obtained different results of dynamic parameters for the LuGre model.

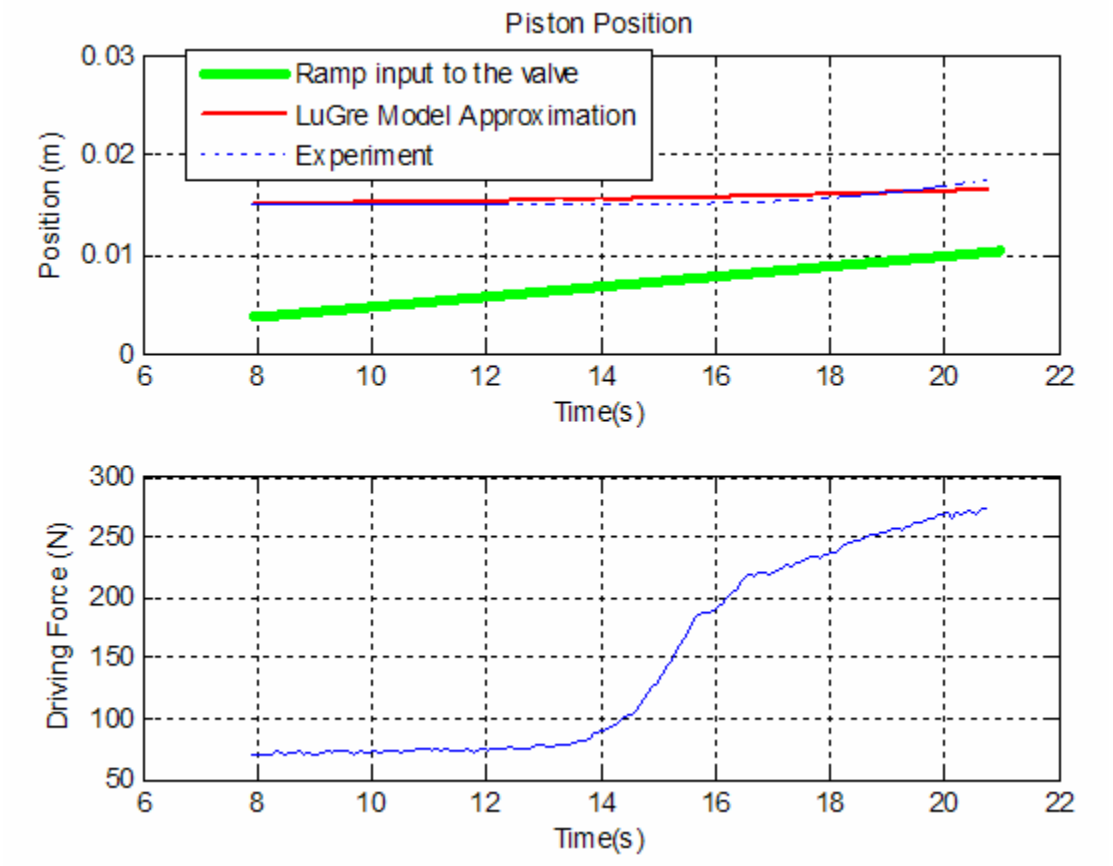

Figure 5.8 Friction estimation using the open loop response of the piston for the initial position of (xp(0)= 0.015 m)

The driving force in figure 5.7 and figure 5.8, is calculated using (5.2), and ramp valve line indicates time change in the ramp input where as the amplitude is arbitrary. As it can be seen from both figures, the approximated response of the piston motion is almost identical to the experimental one.

The bristle stiffness constant is found roughly being the same for many experiments ($\sigma_0 = 4\times10^4$ N/m) while the bristle damping coefficient found to be very sensitive and it varies between (sigma 1 1.64×10^3 N.s/m - 8×10^5 N.s/m) . The uneven distribution of the stiction force along the cylinder can be understood as the direct implication of the variation of the bristles damping coefficient.

5.4 Model Validation

The models described in the previous section such as the valve dynamics, the flow rate equations, pressure dynamics, piston dynamics and the LuGre friction model is implemented in SIMULINK, and open-loop and closed-loop experiments are conducted to validate it. The SIMULINK block diagrams are shown in figure (B.1-B.4).

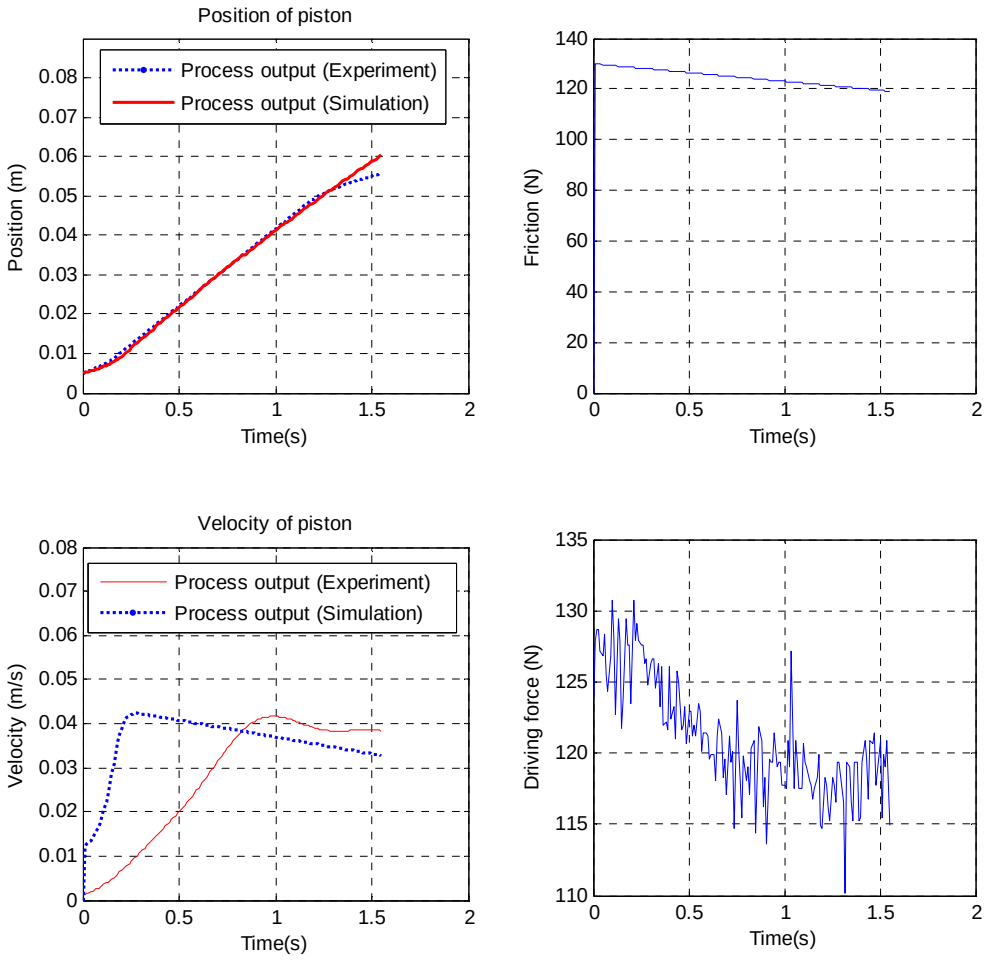

Figure 5.9 Comparison of results obtained from simulation and experiment

The response of the piston position, the velocity, the friction acting on the piston, and the driving force are shown in figure 5.9 for a step input applied to the valve. For the

experiment shown in figure 5.9, the static parameters and the bristle stiffness constant are kept constant as given in table 5.1 while the bristle damping coefficient is changed to 1×10^4 N.s/m, because most of the friction parameter variation observed to be in the bristle damping coefficient.

The assumption made in the identification process of the parameters of the LuGre friction model that the bristles deflection remains constant after the piston motion starts while the bristles deflection rate goes to zero can be verified in figure 5.10.

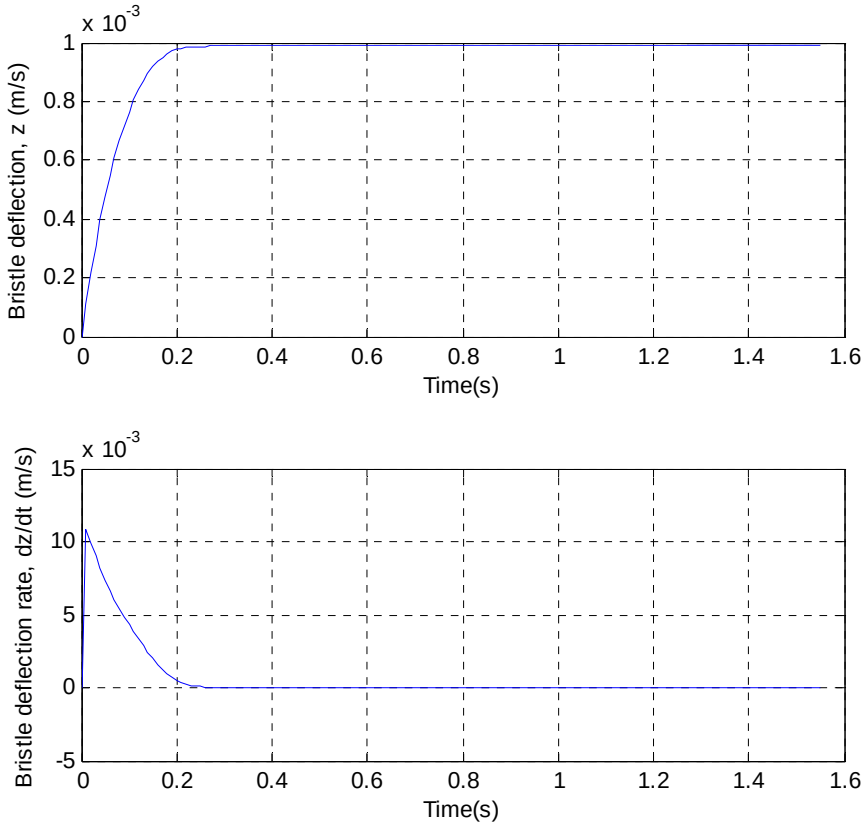

Figure 5.10 Average bristle deflection and deflection rate obtained from experiment for a step input supplied to the valve

The closed loop response of the piston position for a step input of amplitude 0.02 m using a proportional controller of gain 10 is shown in Figure 5.11

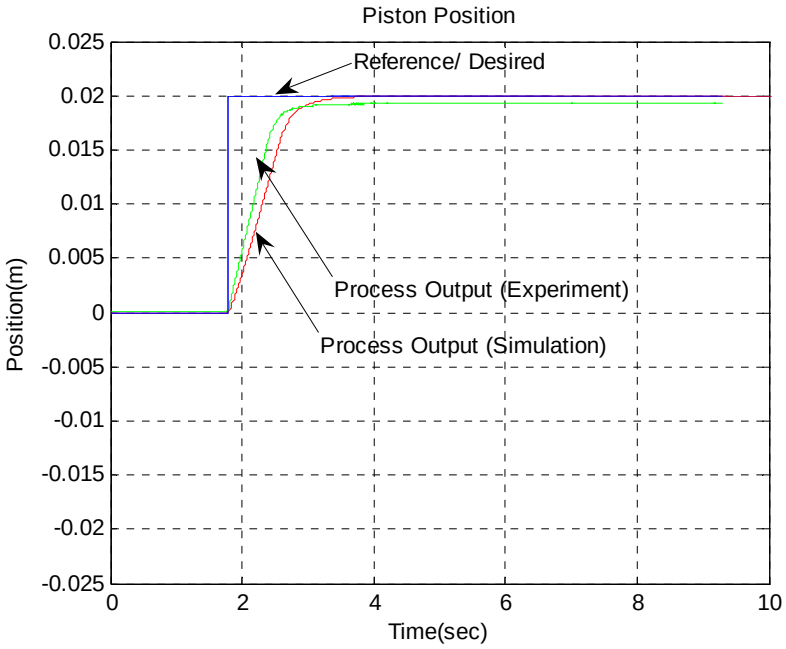

Figure 5.11 Comparison of piston position while tracking the step input in simulation and experiment

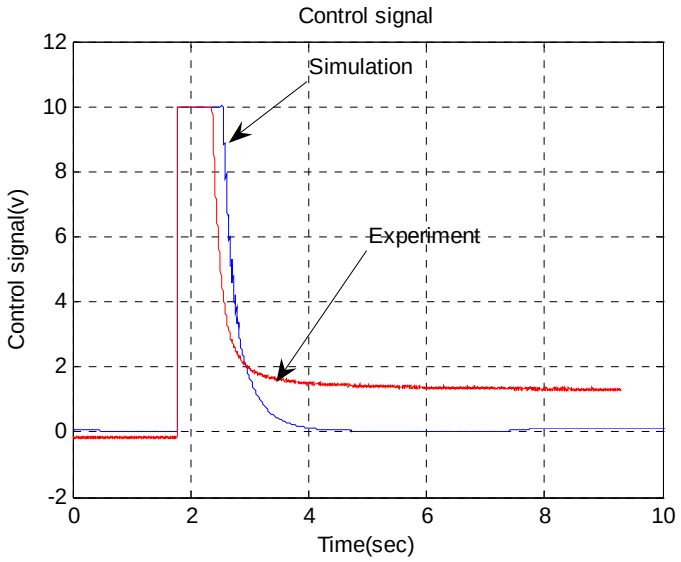

Figure 5.12 Comparison of Control signal (V) for tracking the step input in simulation and experiment

5.5 Conclusions

In this chapter we have presented the identification of the friction parameters by dividing the friction phenomenon into two regions, static parameters and dynamic parameters. The static parameters are determined from the sliding region of the friction-velocity curve. The dynamic parameters are determined from the pre-sliding region of the friction-velocity curve. We have observed that the stiction force is unevenly distributed along the cylinder, and also the damping coefficient of the bristles is very sensitive which varies significantly. The variation of the bristle damping coefficient affects directly the stiction force because the larger the damping coefficient the larger the breakaway force (stiction) needed to deflect or slip the bristles. We have also presented experiments that successfully validated the identified parameters of the LuGre friction model. Again simulation results for some open loop and closed loop responses have shown the validation of both the LuGre friction model and also the hydraulic system model.

CHAPTER VI

NONLINEAR CONTROLLER DESIGN

6.1 Introduction

Modeling inaccuracies can have strong adverse effects on nonlinear control systems. Nonlinear system model imprecision may come from parametric uncertainties and unmodeled dynamics. The first kind corresponds to inaccuracies on the terms actually included in the model, while the second kind corresponds to inaccuracies on the system order. In the previous chapter we have observed that the friction parameters from the LuGre friction model change as a function of position and temperature. Thus it will be necessary to design robust controller that can cope with the friction variations. One of the most important approaches in dealing with this kind of model uncertainty is a robust control. The typical structure of a robust controller is composed of a nominal part, similar to a feedback linearizing, and additional terms aimed at dealing with model uncertainty.

In our approach, the sliding mode robust controller is derived from a Lyapunov analysis of the nonlinear dynamic equations for the proportional valve and hydraulic actuator. The basic form of the control law is obtained similar to those developed by Batur and Jalal [7] for pneumatic systems. Sliding mode control design provides a systematic approach to the problem of maintaining stability and consistent performance in the face of modeling imprecision.

6.2 Sliding Mode Control Philosophy

Sliding mode control gained much popularity in the recent years due to its applicability to non-linear systems and the ability to consider robustness issues in the global sense. Sliding mode control has been successfully applied to robot manipulators, underwater vehicles, automotive transmissions and engines, high-performance electric motors and power systems [16].

Sliding mode control provides a systematic approach to the problem of maintaining stability and consistent performance in the face of modeling imprecision. Sliding mode control systems are a class of systems whereby *the control law* is deliberately changed during the control process according to some defined rules, which depend on the state of the system [16]. According to the control objectives, it constructs a so-called sliding manifold or sliding surface and forces the system states to reach and subsequently remain on within the sliding surface. The sliding surface will be an invariant set by taking the square of the sliding manifold function as a Lyapunov function candidate, and choosing some parameters. Then the dynamic behavior of the system when confined to the surface is described as sliding motion. The complete response of sliding motion control system consists of two distinct phases of motion. The initial phase referred to as the reaching phase where it takes a *finite time* for the state trajectories to reach the sliding surface from any initial condition. The second phase is described by a sliding motion after reaching the sliding surface and moving to the desired state exponentially.

6.3 Sliding Mode Control Development

We will begin the derivation of the control law from the dynamics of the piston motion

$$\ddot{x}_P = \frac{1}{m}\left[P_1 A_1 - P_2 A_2 - mg - F_f\right] \tag{6.1}$$

Differentiating equation (6.1) yields

$$\dddot{x}_P = \frac{1}{m}\left[\dot{P}_1 A_1 - \dot{P}_2 A_2 - \dot{F}_f\right] \tag{6.2}$$

According to equation (3.20) and (3.21) the pressure dynamics in the hydraulic cylinder for negligible leakage flows, $q_{leakage}$ can be written as follows

$$\dot{P}_1 = \frac{\beta}{V_1}(-\dot{V}_1 + q_1) \tag{6.3}$$

$$\dot{P}_2 = \frac{\beta}{V_2}(-\dot{V}_2 - q_2) \tag{6.4}$$

substituting $\dot{P}_1$ and $\dot{P}_2$ from equations (6.3) and (6.4) to (6.2) gives

$$\dddot{x}_P = \frac{1}{m}\left[\frac{\beta A_1}{V_1}(-\dot{V}_1 + q_1) - \frac{\beta A_2}{V_2}(-\dot{V}_2 - q_2) - \dot{F}_f\right] \tag{6.5}$$

rearranging equation (6.5) gives

$$\dddot{x}_P = \frac{1}{m}\left[-\frac{\beta A_1 \dot{V}_1}{V_1} + \frac{\beta A_2 \dot{V}_2}{V_2} - \dot{F}_f\right] + \frac{1}{m}\left[\frac{\beta A_1 q_1}{V_1} + \frac{\beta A_2 q_2}{V_2}\right] \tag{6.7}$$

According to equation (3.17) and (3.18) the flow equations for the hydraulic valve by taking the tank pressure equal to zero can be given as:

$$q_1 = C_v x_v \left(sgn(x_v)\sqrt{P_S - P_1} + sgn(-x_v)\sqrt{P_1}\right), \tag{6.8}$$

$$q_2 = C_v x_v \left(sgn(x_v)\sqrt{P_s - P_2} + sgn(-x_v)\sqrt{P_2}\right), \tag{6.9}$$

substituting equation (6.8) and (6.9) for q_1 and q_2 in (6.7) gives

$$\ddot{x}_P = \left\{\frac{1}{m}\left[-\frac{\beta A_1 \dot{V}_1}{V_1} + \frac{\beta A_2 \dot{V}_2}{V_2} - \dot{F}_f\right]\right\} + \left\{\frac{1}{m}\left[\frac{\beta A_1 C_v (sgn(x_v)\sqrt{P_s - P_1} + sgn(-x_v)\sqrt{P_1})}{V_1}\right]\right.$$

$$\left. + \frac{1}{m}\left[\frac{\beta A_2 C_v (sgn(x_v)\sqrt{P_s - P_2} + sgn(-x_v)\sqrt{P_2})}{V_2}\right]\right\} x_v \qquad (6.10)$$

For the simplicity of the controller design, the relation between the spool position of the valve, x_v and the control input, u is considered instantaneous rather than through dynamic equation (3.6). Since the bandwidth of the valve is large (300 Hz) compared to the bandwidth of whole hydraulic system (2.4 Hz) the above assumption above can be safely made. With this assumption equation (6.10) can be written as:

$$\ddot{x}_P = \left\{\frac{1}{m}\left[-\frac{\beta A_1 \dot{V}_1}{V_1} + \frac{\beta A_2 \dot{V}_2}{V_2} - \dot{F}_f\right]\right\} + \left\{\frac{1}{m}\left[\frac{\beta A_1 C_v (sgn(x_v)\sqrt{P_s - P_1} + sgn(-x_v)\sqrt{P_1})}{V_1}\right]\right.$$

$$\left. + \frac{1}{m}\left[\frac{\beta A_2 C_v (sgn(x_v)\sqrt{P_s - P_2} + sgn(-x_v)\sqrt{P_2})}{V_2}\right]\right\} u \qquad (6.11)$$

Now let's assume equation (6.11) is in the form of

$$\ddot{x}_P = f + bu \qquad (6.12)$$

where u is the control input, the scalar x_P is the output of interest (piston position), the control gain, b is known or measurable and the dynamics, f is a non-linear and not exactly known (uncertainty in friction parameters)

$$f = \frac{1}{m}\left[-\frac{\beta A_1 \dot{V}_1}{V_1} + \frac{\beta A_2 \dot{V}_2}{V_2} - \dot{F}_f\right] \qquad (6.13)$$

Let's define a surface for the single input dynamic system described by equation (6.12) in the state-space by the scalar equation s(x;t) = 0, where

$$s(x,t) = (\frac{d}{dt} + \lambda)^2 \tilde{x} \tag{6.14}$$

$$= (\frac{d^2}{dt^2} + \lambda_1 \frac{d}{dt} + \lambda_2)\tilde{x} \tag{6.15}$$

Where λ_1 (λ_1 =2 λ) and λ_2 ($\lambda_2 = \lambda^2$) are strictly positive constant, whose choice we shall interpret later. The position tracking error, $\tilde{x}$ is defined by

$$\tilde{x} = x_d - x_P \tag{6.16}$$

Where x_d is the set point. The sliding surface, s which is simply a weighted some of the position, velocity and acceleration error can be written as

$$s = \ddot{\tilde{x}} + \lambda_1 \dot{\tilde{x}} + \lambda_2 \tilde{x} \tag{6.17}$$

Taking derivative of equation (6.17) gives

$$\dot{s} = \dddot{\tilde{x}} + \lambda_1 \ddot{\tilde{x}} + \lambda_2 \dot{\tilde{x}} \tag{6.18}$$

$$\Rightarrow \dot{s} = \dddot{\tilde{x}}_d - \dddot{\tilde{x}}_P + \lambda_1 \ddot{\tilde{x}} + \lambda_2 \dot{\tilde{x}} \tag{6.19}$$

Substituting $\dddot{\tilde{x}}_P$ from equation (6.12) to (6.19) we get:

$$\dot{s} = -f - bu + \dddot{\tilde{x}}_d + \lambda_1 \ddot{\tilde{x}} + \lambda_2 \dot{\tilde{x}} \tag{6.20}$$

There are two parts in the control signal, one is the linear part another is the robustness part given by

$$u = u_{linear} + u_{robust} \tag{6.21}$$

The equivalent control is defined as the signal u_{linear} which makes $\dot{s}$ =0. However since f is not exactly known then an approximation would be

$$u_{linear} = \frac{1}{b}(-\hat{f} + \dddot{\tilde{x}}_d + \lambda_1 \ddot{\tilde{x}} + \lambda_2 \dot{\tilde{x}}) \tag{6.22}$$

where $\hat{f}$ is an estimate of f. The uncertainty in f as the result of the friction parameter variations is assumed to be bounded by some known function F from the knowledge of experiments performed in the previous chapter.

$$| \hat{f} - f | \leq F \tag{6.23}$$

Second part of the control signal is the robustness term, which is designed to take care of the uncertainties in f and to force the states to be driven towards the sliding surface. Now choosing

$$u_{robust} = \frac{1}{b(x)}[K \operatorname{sgn}(s)] \tag{6.24}$$

so that the sliding surface becomes attractive, and that can be shown using a Lyapunov function

$$V = \frac{1}{2}s^2 \tag{6.25}$$

Differentiating equation (6.25)

$$\dot{V} = s\dot{s} \tag{6.26}$$

Substituting $\dot{s}$ from equation (6.20) to (6.26) gives

$$\dot{s} = -f - [-\hat{f} + \dddot{\tilde{x}}_d + \lambda_1 \ddot{\tilde{x}} + \lambda_2 \dot{\tilde{x}} + K \operatorname{sgn}(s)] + \lambda_1 \ddot{\tilde{x}} + \lambda_2 \dot{\tilde{x}} + \dddot{\tilde{x}}_d \tag{6.27}$$

$$\Rightarrow \dot{s} = \hat{f} - f - K \operatorname{sgn}(s) \tag{6.28}$$

Which results in,

$$\dot{V} = s(\hat{f} - f) - K | s | \tag{6.29}$$

From the definition of F in (6.23) we can write (6.29) as

$$\dot{V} \leq F \mid s \mid -K \mid s \mid \tag{6.30}$$

So that, by letting

$$K = F + \eta, \tag{6.31}$$

we get

$$\dot{V} \leq -\eta \mid s \mid \tag{6.32}$$

Where $\eta > 0$, thus it constraints trajectories to point towards the sliding surfaces. If $s = 0$ then the derivative of the Lyapunov function ($\dot{V} = 0$) which implies the trajectories may or may not leave the sliding surface but if they leave the sliding surface $(s \neq 0)$ again they will be forced to go back too the surface. Satisfying the sliding condition makes the surface an invariant set (a set for which any trajectory starting from an initial condition within the set remains in the set for all future times). Furthermore equation (6.32) implies that some disturbances or dynamic uncertainties can be tolerated while still keeping the surface an invariant set. The use of *sgn(s)* in equation (6.24) creates chattering which is undesirable, and in practice the high control activity can possibility excite unmodeled high frequency dynamics (e.g. the proportional valve).

6.4 Chattering Reduction

We know that the control law has to be discontinuous across $s = 0$ in order to account for the present modeling imprecision and disturbances. Since the implementation of the associated control switching is necessarily imperfect (for instance, in practice the presence of finite time delays for control computation and the limitation of physical actuators), chattering is undesirable in practice, since it involves high control activity and

may further excite the unmodeled dynamics of the system [16]. In general chattering must be eliminated for the controller to perform properly. This can be achieved by smoothing out the control discontinuity in a thin boundary layer neighboring the switching surface.

To minimize chattering in the controller, we can use a saturation function defined by

$$\text{sat}(s) = s, \qquad \text{if } |s| \le 1 \tag{6.33}$$

$$= sgn(s), \qquad \text{if } |s| > 1$$

We can approximate the *sign* non-linearity by a saturation non-linearity with high slope

$$sgn(s) \approx \text{sat}(\frac{s}{\varepsilon}) \tag{6.34}$$

where ε is a positive constant, and for good approximation of (6.34) ε has to be very small. However, when ε is too small, the high gain feedback in the linear portion of the saturation function may excite unmodelled high-frequency dynamics. Therefore the choice of ε is a tradeoff between accuracy and exciting unmodeled high frequency dynamics. On the contrary, a large ε will reduce the accuracy while smoothing the control signal. In the limit, as $\varepsilon \to 0$, the saturation non-linearity $\text{sat}(\frac{s}{\varepsilon})$ approaches the sign non-linearity *sgn*(s) as shown in figure 6.2.

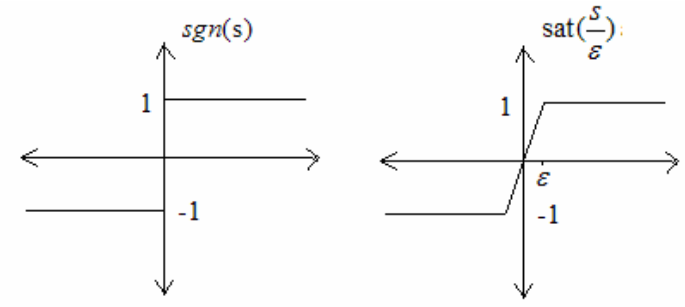

Figure 6.1 Sign non-linearity and saturation function

Now using

$$u_{robust} = \frac{1}{b}[K\text{sat}(\frac{s}{\varepsilon})] \tag{6.35}$$

where,

$$\text{sat}(\frac{s}{\varepsilon}) = \frac{s}{\varepsilon}, \qquad \text{if } |\frac{s}{\varepsilon}| < 1 \text{ or } |s| < \varepsilon \tag{6.36}$$

$$= sgn(\frac{s}{\varepsilon}), \quad \text{if } |\frac{s}{\varepsilon}| \geq 1 \text{ or } |s| \geq \varepsilon$$

To analyze the stability of the system, we use the Lyapunov function

$$V = \frac{1}{2}s^2 \tag{6.37}$$

$$\dot{V} = s\dot{s} \tag{6.38}$$

Using equation (6.35) and substituting in (6.20)

$$\dot{s} = -f - [-\hat{f} + \dddot{\tilde{x}}_d + \lambda_1\ddot{\tilde{x}} + \lambda_2\dot{\tilde{x}} + K\text{sat}(\frac{s}{\varepsilon})] + \lambda_1\ddot{\tilde{x}} + \lambda_2\dot{\tilde{x}} + \dddot{\tilde{x}}_d \tag{6.39}$$

$$\Rightarrow \dot{s} = \hat{f} - f - K\text{sat}(\frac{s}{\varepsilon}) \tag{6.40}$$

Which gives,

$$\Rightarrow \dot{V} = s[\hat{f} - f] - s[K\text{sat}(\frac{s}{\varepsilon})] \tag{6.41}$$

$$\dot{V} \leq F|s| - s[K\text{sat}(\frac{s}{\varepsilon})] \tag{6.42}$$

So that by letting $K = F + \eta$, in the region $|s| \geq \varepsilon$, we have

$$\dot{V} \leq F|s| - [F + \eta]\text{sgn}(\frac{s}{\varepsilon}).s \tag{6.43}$$

Knowing $\text{sgn}(\frac{s}{\varepsilon}).s = |s|$

$$\dot{V} \leq -\eta \mid s \mid \tag{6.44}$$

Which shows that whenever $| s | \geq \varepsilon$, *s(t)* will be strictly decreasing until it reaches the set $\{| s | \leq \varepsilon\}$ in finite time and remains thereafter. The set $\{| s | = \varepsilon\}$ defines two planes where the system states stay between the two planes $s = \varepsilon$ and $s = -\varepsilon$.

The choice of η also determines the *finite time* it takes to reach for the state trajectories starting from any initial condition ($s(t=0)$) to the sliding surface. Integrating equation (6.44) for $s > 0$ between $t = 0$ and $t = t_r$ gives

$$s(t_r) - s(0) \leq -\eta \, . \, t_r \tag{6.46}$$

Where t_r is the time to reach the sliding surface and knowing $s(t_r) = 0$

$$t_r \leq \frac{s(0)}{\eta} \tag{6.45}$$

One would obtain a similar result starting from $s < 0$, and thus

$$t_r \leq \frac{| s(0) |}{\eta} \tag{6.47}$$

Starting from any initial condition, the state trajectory reaches the sliding surface in a finite time smaller than $\frac{| s(0) |}{\eta}$.

6.5 Transient and Steady State Response

The time response of a control system consists of two parts: the transient response and the steady state response. The transient response corresponds to the system output just after the system is turned on for a short period of time. If the system is asymptotically stable, the transient response disappears otherwise the transient response increase if the

system is unstable. The steady state response corresponds to the difference between the desired and the actual output of the system at steady state.

After the sliding mode control makes sure that s goes to zero, equation (6.17) becomes

$$\ddot{\tilde{x}} + \lambda_1 \dot{\tilde{x}} + \lambda_2 \tilde{x} = 0 \tag{6.45}$$

Which represents a linear differential equation whose steady state solution exponentially goes to zero ($\tilde{x}$ =0) . The choice of λ_1 and λ_2 imply the speed of the transient response of the system. The characteristics of the transient response of the system such as delay time, rise time, maximum overshoot and settling time to a step input can be designed by changing λ_1 and λ_2 .

6.6 Conclusions

This chapter presents briefly the design of the sliding mode controller for the hydraulic system. A suitable Lyapunov function candidate is selected to force the state trajectories to reach the sliding manifold in finite time and also to remain there. The implementation of sliding mode controller by control switching is necessarily imperfect and produces chattering. The chattering phenomenon in the sliding mode control is eliminated by introducing a thin boundary layer around the sliding surface, and as a result, a smooth control signal can be generated. The performance of the proposed controller is experimentally demonstrated in the next chapter.

CHAPTER VII

POSITION TRACKING THROUGH SIMULATION AND EXPERIMENT

7.1 Introduction

The proposed sliding mode control is implemented in MATLAB/SIMULINK and carried out using the Math Works Real-Time Workshop connected to dSPACE 1104 signal processor board around TMS320C31 floating point DSP which includes onboard A/D and D/A converters. The parameters of the controller implemented are changed and monitored through ControlDesk software in real-time. A block diagram of the hydraulic control system used for simulation is shown in figure 7.1. The detailed mathematical model of each block diagram used in SIMULINK is found in figures (B.1 - B.5)

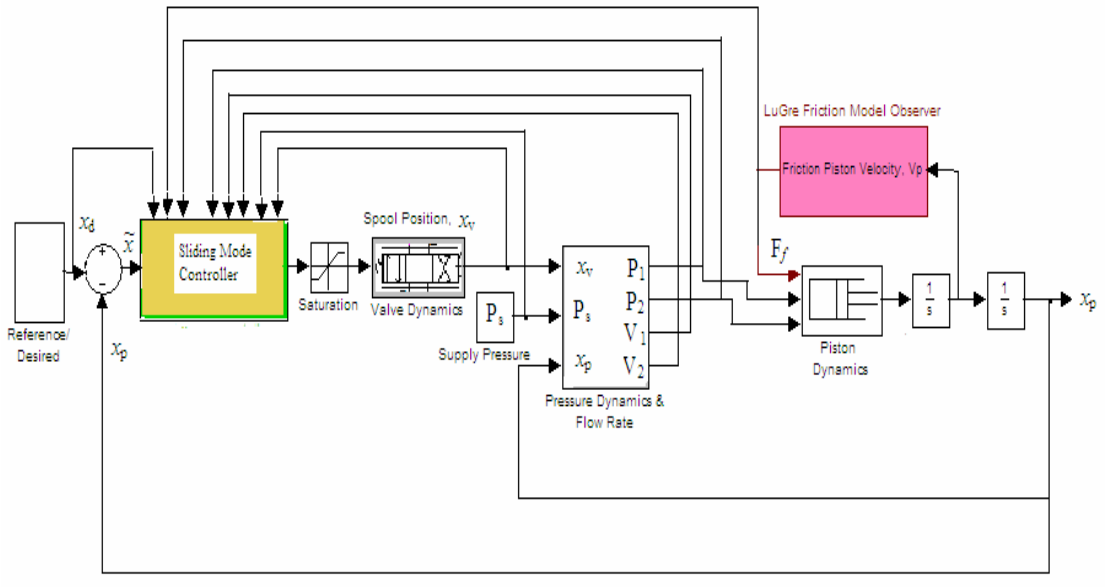

Figure 7.1 Closed loop hydraulic system control

The inputs for the sliding mode controller during experiment are obtained from the measurement of the piston position, x_p , the pressure from the bottom and upper chamber of the cylinder, and the spool position, x_v, while the friction is predicted using the LuGre model which takes the velocity measurement of the piston into account. The velocity of the piston is obtained by taking the derivative of the piston position signal and passing it through a low pass filter ($\frac{1}{0.4s+1}$) to reduce the noise in the velocity signal. The time constant used for the low pass filter is chosen carefully from the knowledge of the bandwidth of the system obtained from chapter III so that important velocity signal is not lost.

To effectively assess the performance of the proposed sliding mode control, several experiments and simulations have been performed with different desired inputs and sliding mode controller parameters. A step and sine wave inputs are used to evaluate position tracking ability of the piston. However different transient response of the hydraulic piston to a step input has been considered by changing the controller parameters.

7.2 Sliding Mode Controller (switching)

We first proposed in the previous chapter a switched sliding mode Controller where the control signal has to be discontinuous across s = 0 (sign function). Several model based simulations are performed to evaluate the performance of the switched sliding mode controller before implementing it on the hydraulic system. Figures 7.2 – 7.4 represent the response for the piston to a step input of amplitude 20 mm.

The controller parameters are chosen ($\lambda_1 = 8$, $\lambda_2 = 32$, η=10000) so that the transient response characteristics of the system will have a fair overshoot (damping ratio, ζ=0.7) and settling time of one second.

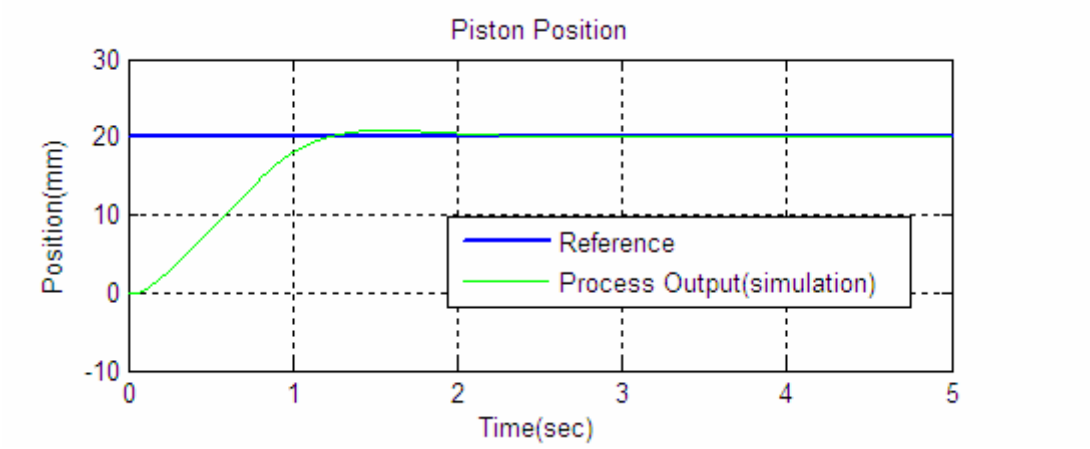

Figure 7.2 Piston position while tracking the step input of amplitude 20 mm (simulation)

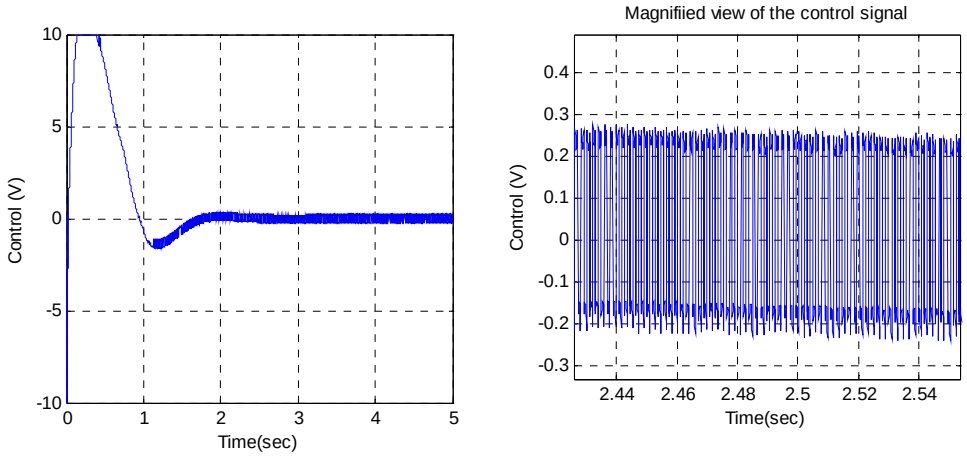

Figure 7.3 Control input and the magnified view to show chattering phenomenon

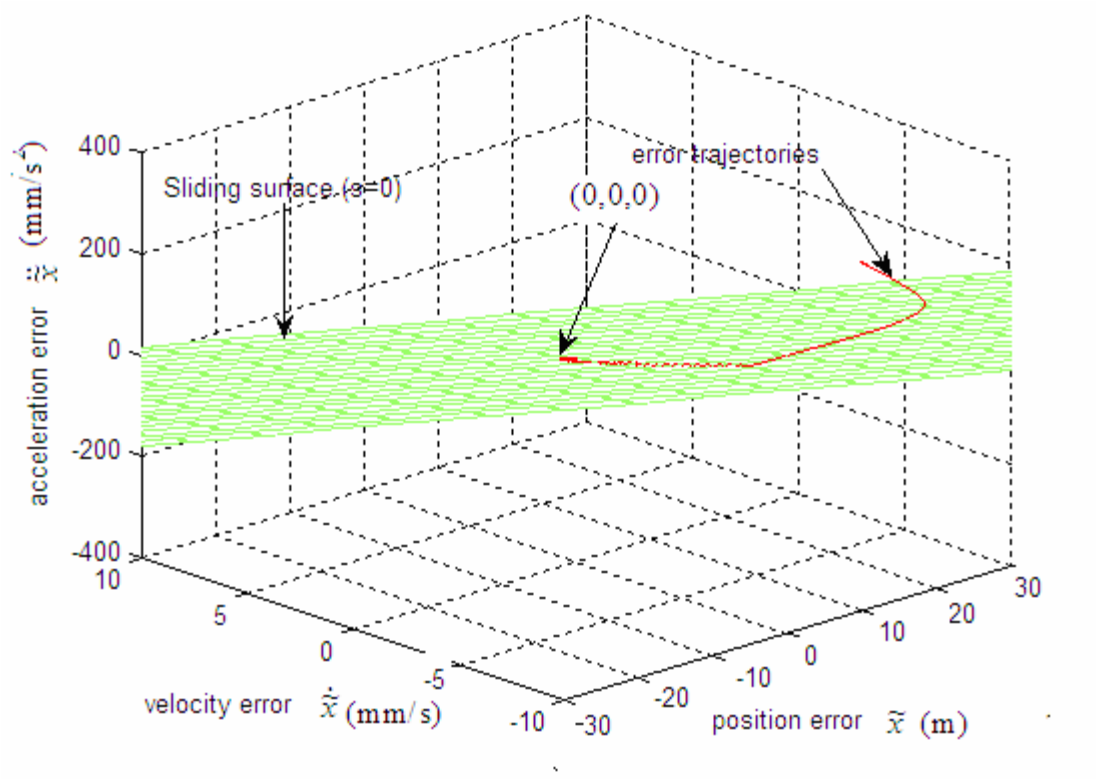

Figure 7.4 Position error trajectories sliding on the sliding manifold (s=0)

Referring to figure 7.2, position response of the piston from the simulation catches the desired position at about one second and with no steady state error. However, fluctuation of the control signal is almost the same with sampling frequency used for the simulation. This kind of control chattering is not practical and cannot be implemented on the hydraulic system. Figure 7.4 explains the motion of the error trajectories starting from ($\tilde{x}$ =20 mm) and getting attracted to the sliding surface in a finite time. It can also be observed that the error trajectories go to zero at steady state.

7.3 Smooth Sliding Mode Controller

Smooth sliding mode controller represents the modified sliding mode controller in the previous chapter for the purpose of reducing chattering (saturation function). As it is shown in figure 7.3 the implementation of control switching is necessarily imperfect due to the limitation of physical actuators and can also excite unmodeled dynamics.

7.3.1 Step Response

Figures 7.5 – 7.8 represent the response for the step input of amplitude 20 mm. The controller parameter are chosen to be the same as before except the new boundary thickness parameter, ε which acts as the boundary plane for the error trajectories (invariant set) . The boundary thickness, ε is chosen to be 0.1.

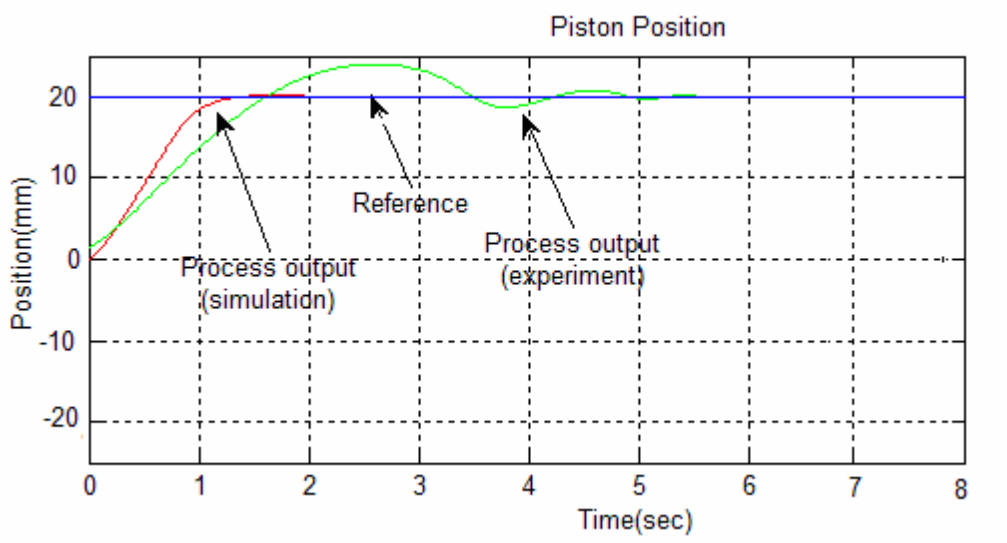

Figure 7.5 Comparison of piston position while tracking the step input in simulation and experiment

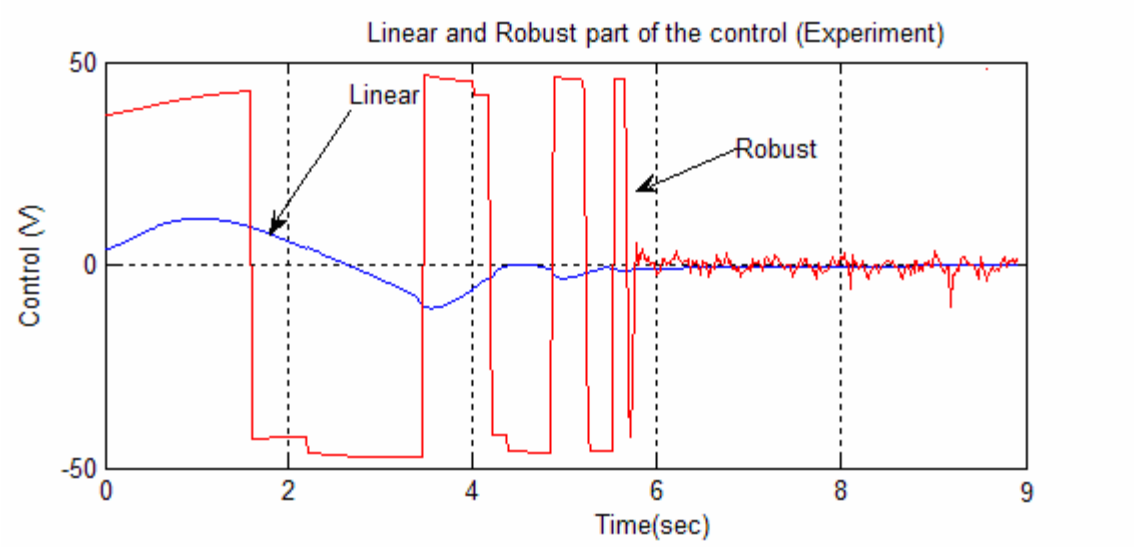

Figure 7.6 Linear and robust part of the Control signal (V)

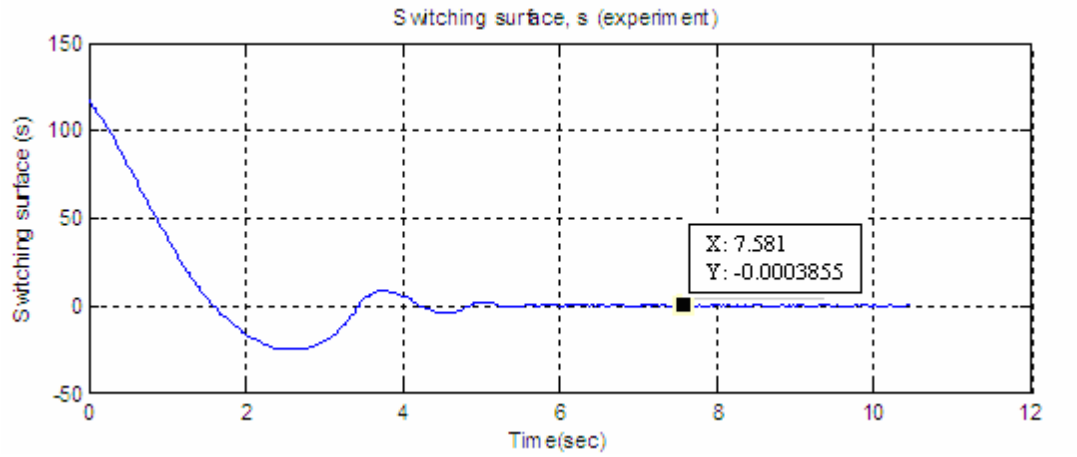

Figure 7.7 Switching surface (s) while tracking the step input (experiment)

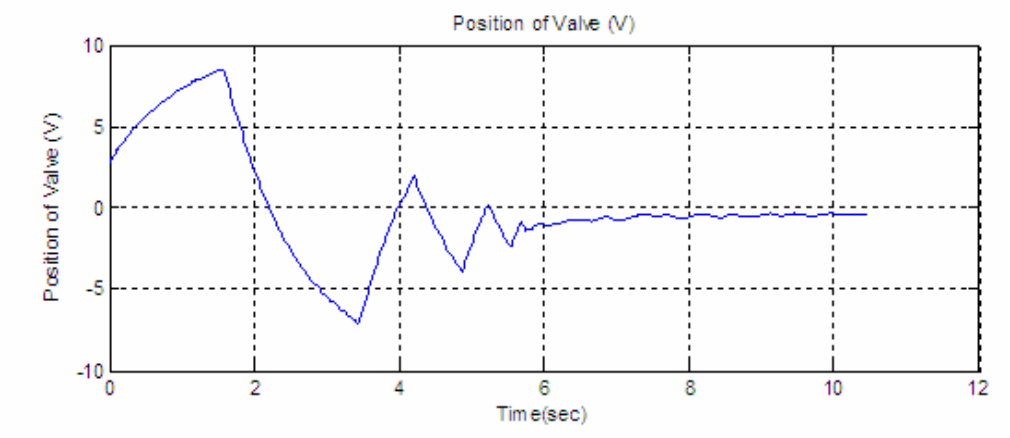

Figure 7.8 Position of the valve for tacking the step input

The boundary thickness, ε is chosen to be very small to maintain good position tracking. The chattering in the control signal is reduced while sustaining the desired position as shown in figures 7.5 and 7.6. The sliding surface function, *s* goes to zero and stays around zero as shown in figure 7.8 which implies the error trajectories are getting close to zero too. The position of the valve did not go to zero even after the piston reached the desired position and that is because the bottom and top chamber of the cylinder have different areas. Therefore to compensate for the different cylinder chamber areas the valve has to allow more fluid to one side.

7.3.2 Sine Wave Response

Experiments and simulations are also done for a sinusoidal wave input of frequency 0.5 rad/s, phase angle of $\pi/4$ and of amplitude 20 mm. The results obtained from experiment and simulations for tracking sinusoidal wave are shown in figures 7.10- 7.13. The boundary thickness of the sliding mode parameter is selected to be very small ($\varepsilon = 0.1$) to have a good tracking accuracy and η is made a large number ($\eta = 50000$) so it will take very small amount of time to reach the sliding surface and also taking care of the uncertainty in friction. Recalling equation 6.43, the derivative of Lyapunov function will be negative or equal to zero if η is chosen to be large satisfying the sliding condition making the surface an invariant set for the error trajectories.

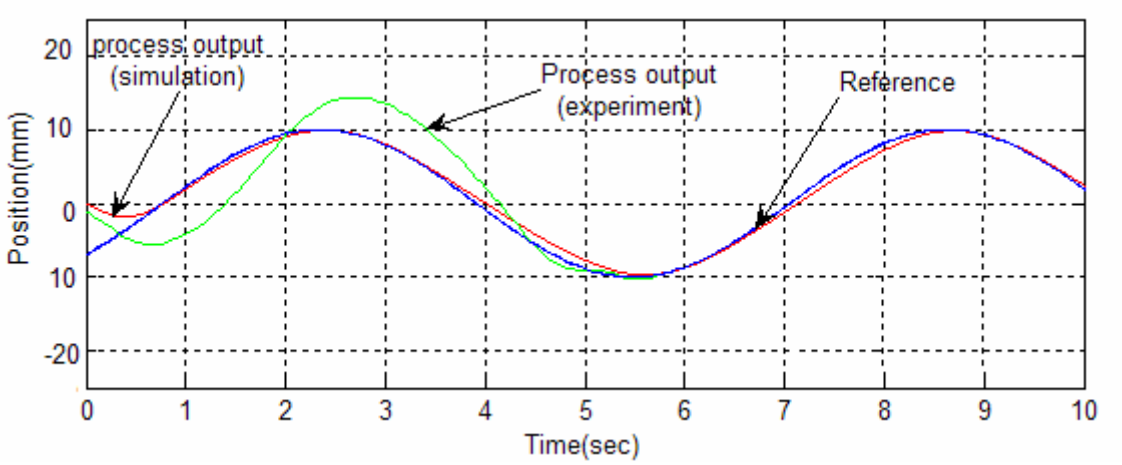

Figure 7.9 Position of the piston for tracking sine wave input (experiment and simulation)

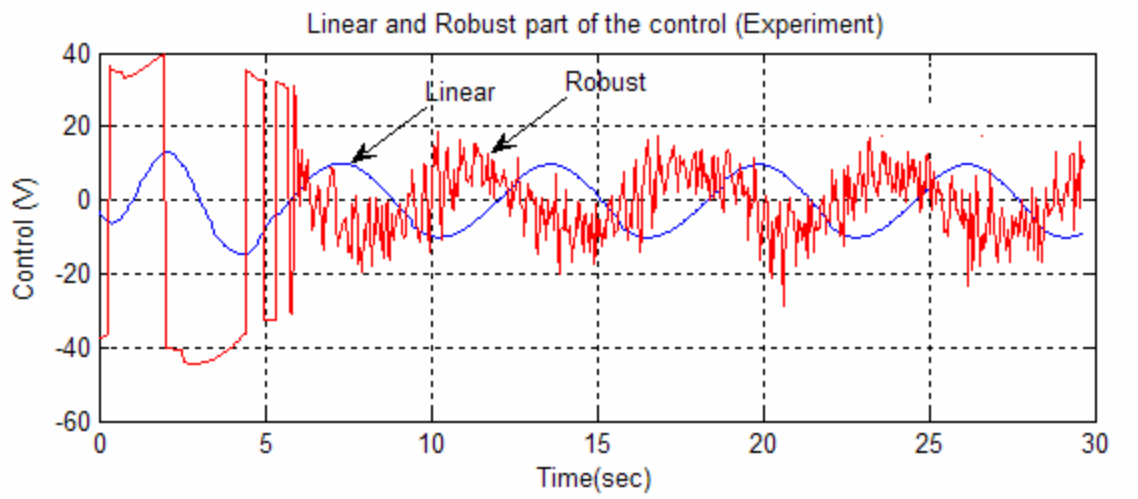

Figure 7 10 Linear and robust part of the Control signal (V)

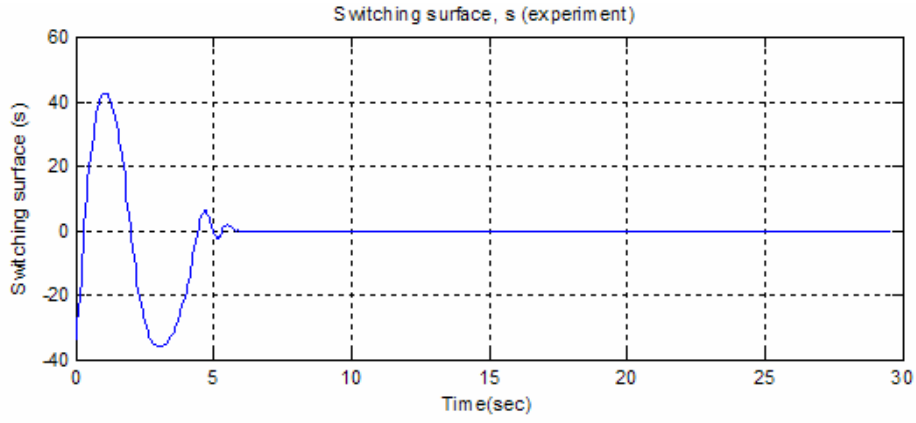

Figure 7.11 Switching surface (s) while tracking the sine wave (experiment)

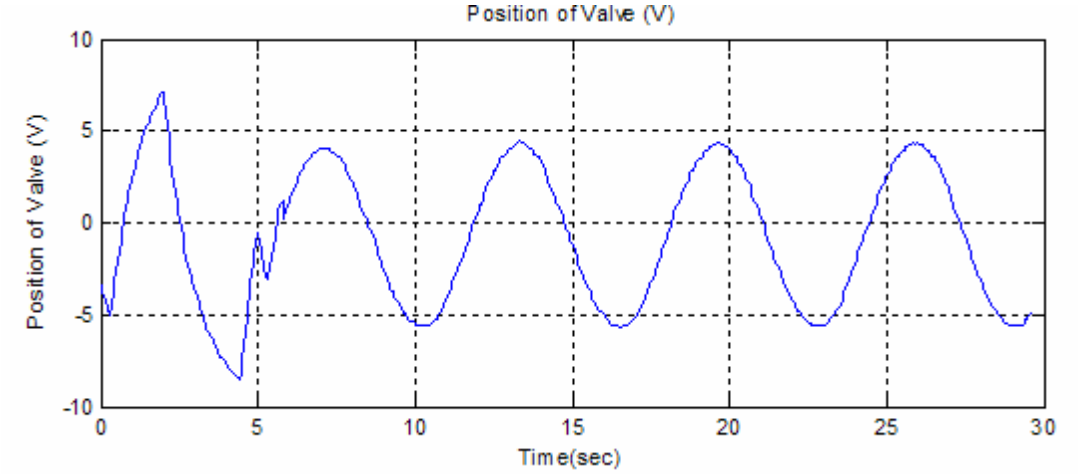

Figure 7.12 Position of the valve for tacking the sine wave input

7.4 Conclusions

This chapter has presented simulated results as well as experimental results for the closed loop hydraulic system. The results obtained in simulation and experiment did not match in the transient period and that is because in simulation we used the averaged value of the identified friction parameters. However friction parameters change extensively as function of position and temperature as demonstrated in chapter V. Secondly, the initial conditions of the pressure in the bottom, pressure in the upper chamber of the cylinder and also the bristle deflection are taken to be zero in simulation but actually in the experiment it did not start from zero. The sliding mode controller in the experiment has demonstrated good position tracking even in the presence of parametric uncertainties in friction. The chattering phenomenon has been reduced while maintaining good position tracking accuracy.

CHAPTER VIII

SUMMARY AND FURTHER RESEARCH

8.1 Summary

This thesis developed and implemented a sliding mode controller for the task of tracking position of a hydraulic system. The analytical and experimental modeling of the hydraulic system is developed in Chapter III. System identification methods by frequency, step and pulse response methods are used to determine the transfer function for the valve and the piston. Analytical models for the flow rate through the valve and pressure dynamics are also developed.

The progress and the development of friction from static to dynamic models have been studied in Chapter IV. Identification of the friction parameters have been performed by dividing the friction phenomenon into two regions, static parameters and dynamic parameters. The static parameters are determined from the sliding region of the friction-velocity curve. The dynamic parameters are determined from the pre-sliding region of the friction-velocity curve. Experiments that successfully validated the identified parameters of the LuGre friction model and also the hydraulic system model have been presented in Chapter V. In applications with high precision positioning and with low velocity tracking a better description of the friction phenomenon using the dynamic model is necessary because at low velocities friction is described well.

In Chapter VI the design of the sliding mode controller for the hydraulic system using a suitable Lyapunov function candidate is developed to force the state trajectories to reach to the desired state. Chattering phenomenon in the sliding mode control is eliminated by introducing a thin boundary layer around the sliding surface, and as a result, a smooth control signal has been generated. Finally, simulated results as well as experimental results for the closed loop hydraulic system using the sliding mode controller have shown good position tracking even in the presence of parametric uncertainties in friction.

8.2 Further Research

The results observed in the previous chapters specifically in the friction parameters which change as a function of position and temperature is the major cause of the hydraulic model uncertainty. The friction parameters have been identified in off-line estimation method in chapter IV. However the same parameter estimation can be made on-line by using adaptive control instead of using the off-line averaged parameters for the friction model. The basic idea in adaptive control is to estimate the uncertain parameters on-line based on the measured input-output data from a plant. Therefore, adaptive control can be used to automatically estimate the friction parameters and as a result obtain a good model.

REFERENCES

[1] C. Canudas de Wit, P. Noel, A. Aubin, and B. Brogliato, Adaptive Friction Compensation in Robot Manipulators: Low Velocities. *Int. J. Rob. Res.,* Vol. 10, No. 3, pp. 189-199, 1991.

[2] C. Canudas de Wit, H. Olsson, K.J. Astrom, and P. Lischinksy, A New Model for Control Systems with Friction. *IEEE Trans Aut. Cntrl.,* Vol. 40, No. 3, pp. 419-425, 1995.

[3] Ayalew, Beshawired and Kulakowski, Bohdan T., Modeling Supply and return Line Dynamics for an Electohydraulic Actuation System. *ISA Transactions*, Vol. 44, No. 3, pp. 329-343, July 2005.

[4] D.A. Haessig and B. Friedland, On the Modeling and Simulation of Friction. *J Dyn Syst Meas Control Trans ASME*, Vol. 113, No. 3, pp. 354-362, September 1991.

[5] C. Canudas de Wit, H. Olsson, K.J. Astrom, P. Lischinksy and M. Gafcert, Friction Models and Friction Compensation. *European Journal of Control*, No.4, pp.176-195, , Dec. 1998.

[6] Jelali, M. and Kroll, A., Hydraulic Servo-systems: Modeling, Identification and Control (Advances in Industrial Control). Springer-Verlag, London, 2003.

[7] Jalal, Syed Shah, Modeling, Study, Analysis and Sliding Mode Control Of A Pneumatic System. Ms Thesis, Department of Mechanical Engineering, The University of Akron, 2003.

[8] Ogata, Katsuhiko, Modern Control Engineering. Prentice Hall, 2002.

[9] Canudas de Wit, H. Olsson, K.J. Astrom, P. Lischinksy. Adaptive Friction Compensation with Partially Known Dynamic Friction Model", *International Journal of Adaptive Control and Signal Processing*, VOL. 11, 65-80 (1997).

[10] Parker Hannifin Corporation, Hydraulic Valve Division, Elyria, Ohio, 44035 USA http://www.parker.com.

[11] P.R. Dahl, A Solid Friction Model. Technical Report TOR-0158(3107-18)-1, The Aerospace Corporation, El Segundo, CA, 1968.

[12] W. Ramberg and W. R. Osgood, Description of Stress-Strain Curves by Three Parameters. Tech. Note 902, National Advisory Committee for Aeronautics, Washington, 1943.

[13] Lancaster, P. and Salkauskas, K., Curve and Surface Fitting: An Introduction. London: Academic Press, 1986.

[14] Gianni Ferretti, Gianantonio Magnani, Gianpaolo Martucci, Friction Model Validation in Sliding and Presliding Regimes with High Resolution Encoders. Control Techniques S.P.A., Via Brodolini 7, 20089, Rozzano, Italy.

[15] Owen, S. William, Reducing Stick-Slip Friction in Hydraulic Actuators, Industrial Automation Laboratory, University of Columbia, 1990.

[16] Slotine Jean-Jacques E., and Li Weiping, Applied Nonlinear Control. Prentice Hall, 1991.

[17] Garett A. Sohl and James E. Bobrow, Experiments and Simulations on the Nonlinear Control of a Hydraulic Servosystem, Department of Mechanical and Aerospace Engineering at the University of California, Irvine, 1999.

[18] Vincent Lampaert, Farid Al-Bender, Jan Swevers, A Generalized Maxwell-Slip Friction Model appropriate for Control Purposes. *Proceedings of the IEEE international conference on Physics and Control,* 2003.

APPENDICES

APPENDIX A

FREQUENCY RESPONSE EXPERIMENT

Experimental values obtained for identification of transfer function of the valve and the piston using frequency response method is found in Table A.1 and A.2.

Table A.1 Experimental frequency response data for the proportional valve

Sine wave Input to Valve		Valve Output	
Freq(Hz)	Amplitude (V)	Amplitude (V)	Phase shift (deg.)
0.050	5	5	0
0.070	5	5	0
0.080	5	5	0
0.090	5	5	0
0.100	5	5	0
0.200	5	5	0
0.300	5	5	0
10	0.5	0.511	0
20	0.5	0.511	-6.47
35	0.5	0.511	-11.32
43	0.5	0.511	-16.9
58	0.5	0.507	-24
69	0.5	0.49	-27
84	0.5	0.48	-30.2
103	0.5	0.476	-33.75
112	0.5	0.471	-36.8
119	0.5	0.47	-38.6
140	0.5	0.456	-50
155	0.5	0.452	-55
171	0.5	0.451	-61
202	0.5	0.43	-72
221	0.5	0.418	-73
240	0.5	0.4	-77
258	0.5	0.383	-83
274	0.5	0.3735	-90
284	0.5	0.3715	-92
300	0.5	0.356	-98.2
315	0.5	0.348	-104

Continued from Table A.1

Sine wave Input to Valve		Valve Output	
Freq(Hz)	Amplitude (V)	Amplitude (V)	Phase shift (deg.)
345	0.5	0.322	-112
368	0.5	0.3015	-116
382	0.5	0.305	-124
395	0.5	0.303	-134
410	0.5	0.28	-144

Table A.2 Experimental frequency response data for the piston

Sine wave Output from Valve		Piston Output	
Freq(Hz)	Amplitude (V)	Amplitude (V)	Phase shift (deg.)
0.050	5	4.35	-90
0.070	5	2.694	-90
0.080	5	2.39	-90
0.090	5	1.94	-90
0.100	5	1.72	-90
0.200	5	0.87	-90
0.300	5	0.625	-90

APPENDIX B

HYDRAULIC CONTROL SYSTEM IN SIMULINK

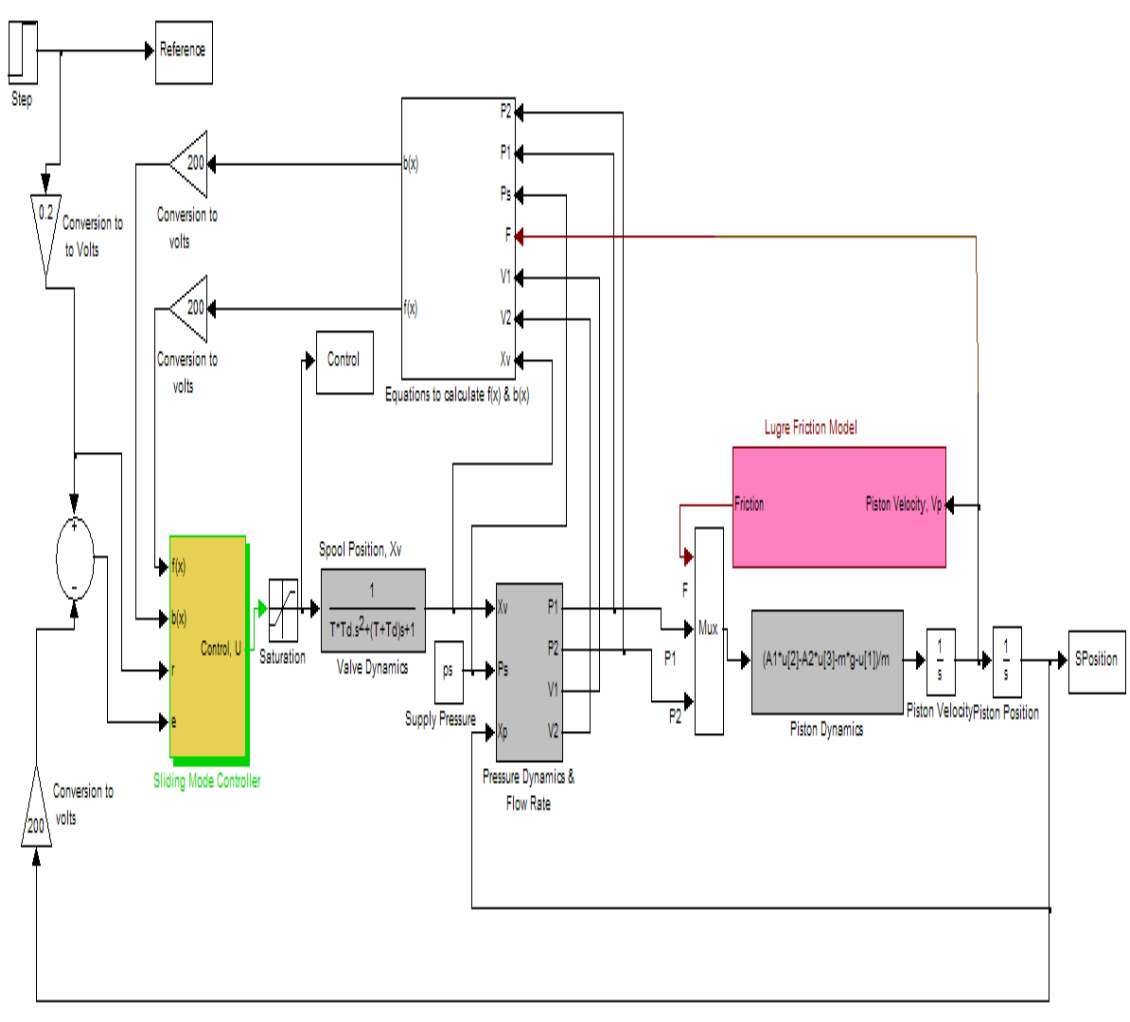

Figure B.1 Closed loop hydraulic system used in SIMULINK

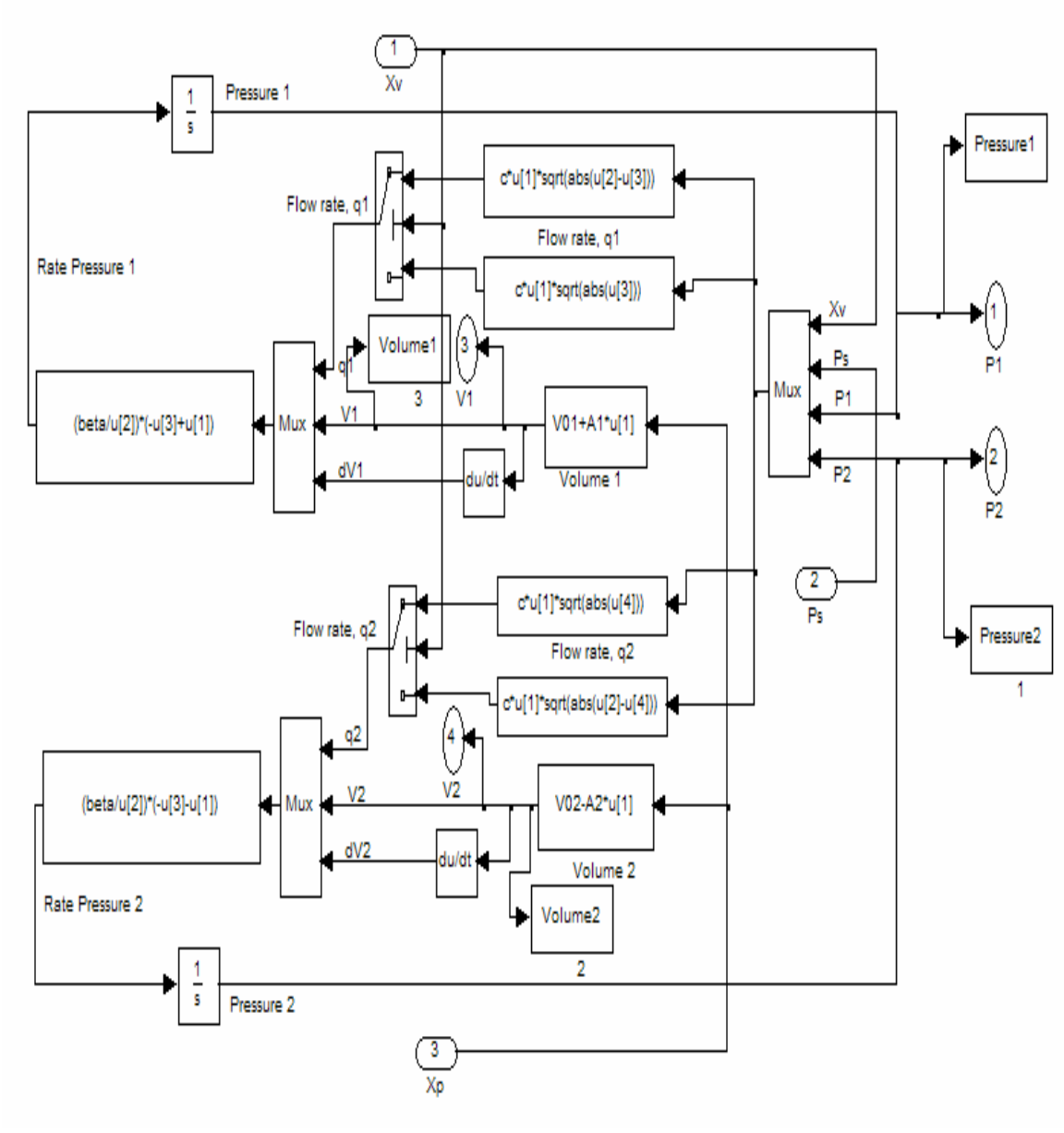

Figure B.2 SIMULINK block diagram used to calculate pressure dynamics and flow rate

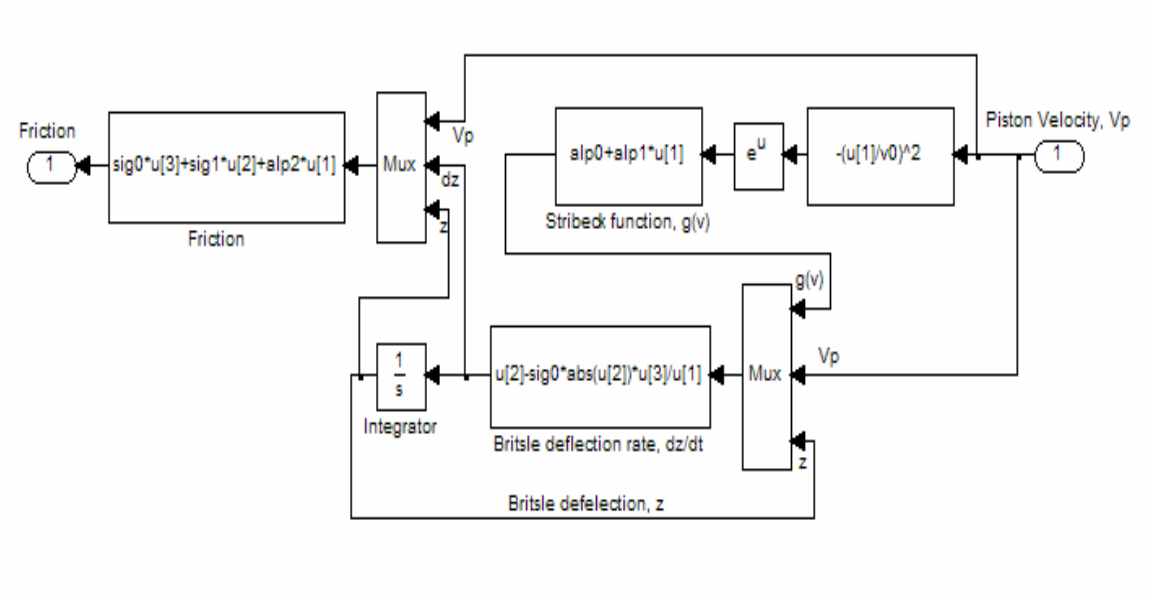

Figure B.3 SIMULINK block diagram used to model LuGre friction model

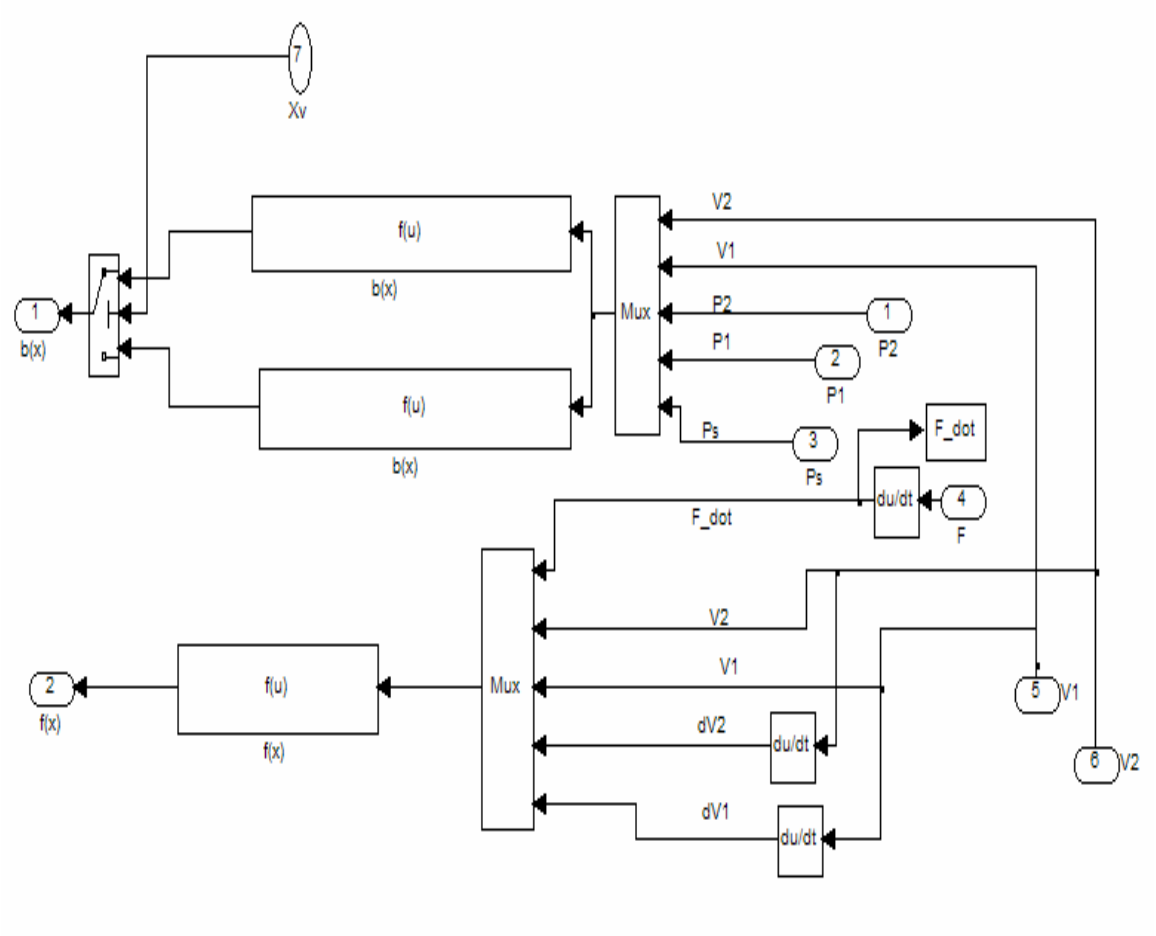

Figure B.4 SIMULINK block diagram used to calculate f and b for the sliding mode controller

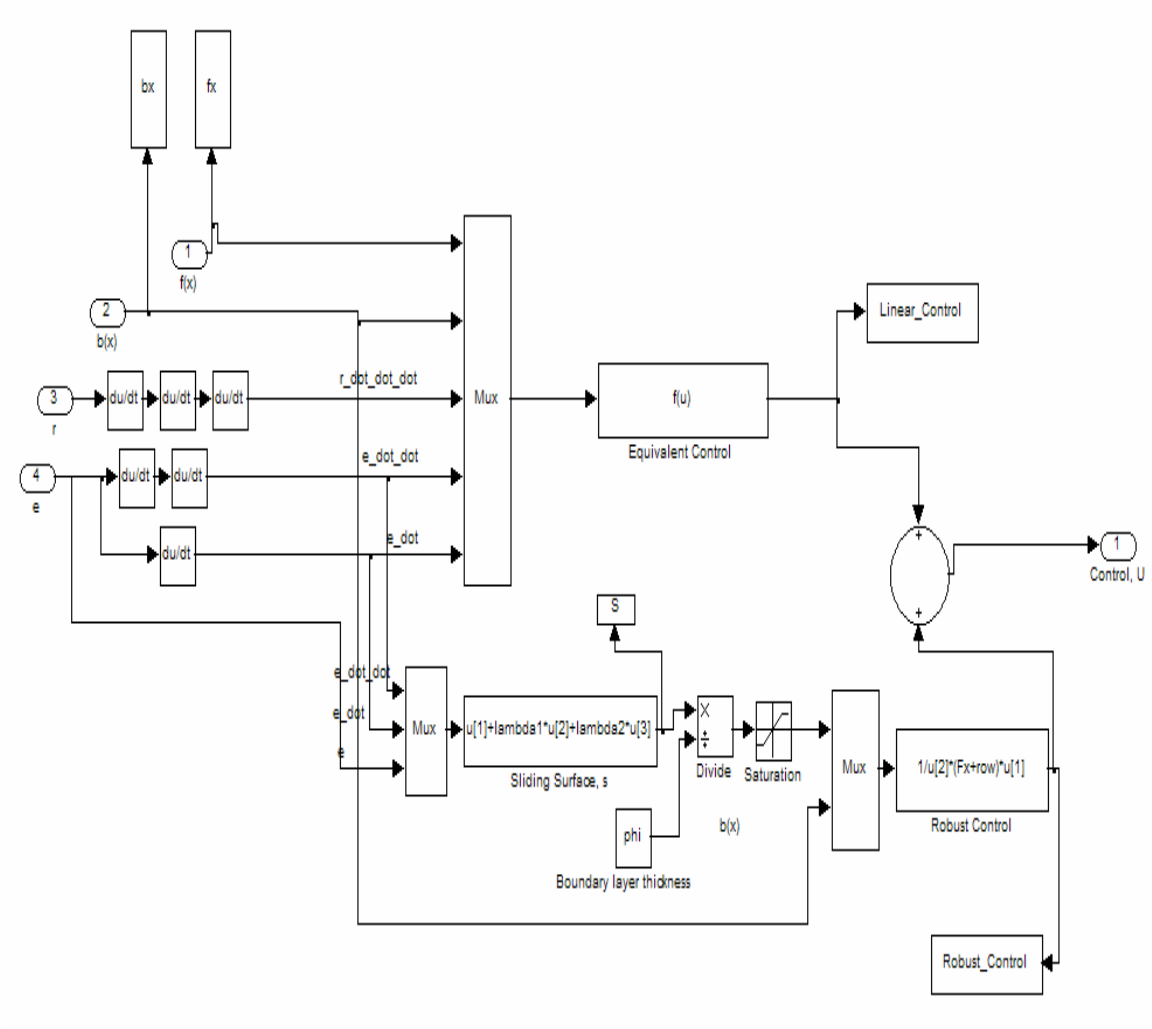

Figure B.5 Sliding mode controller model in SIMULINK

APPENDIX C

EXPERIMENTAL SETUP OF THE HYDRAULIC SYSTEM

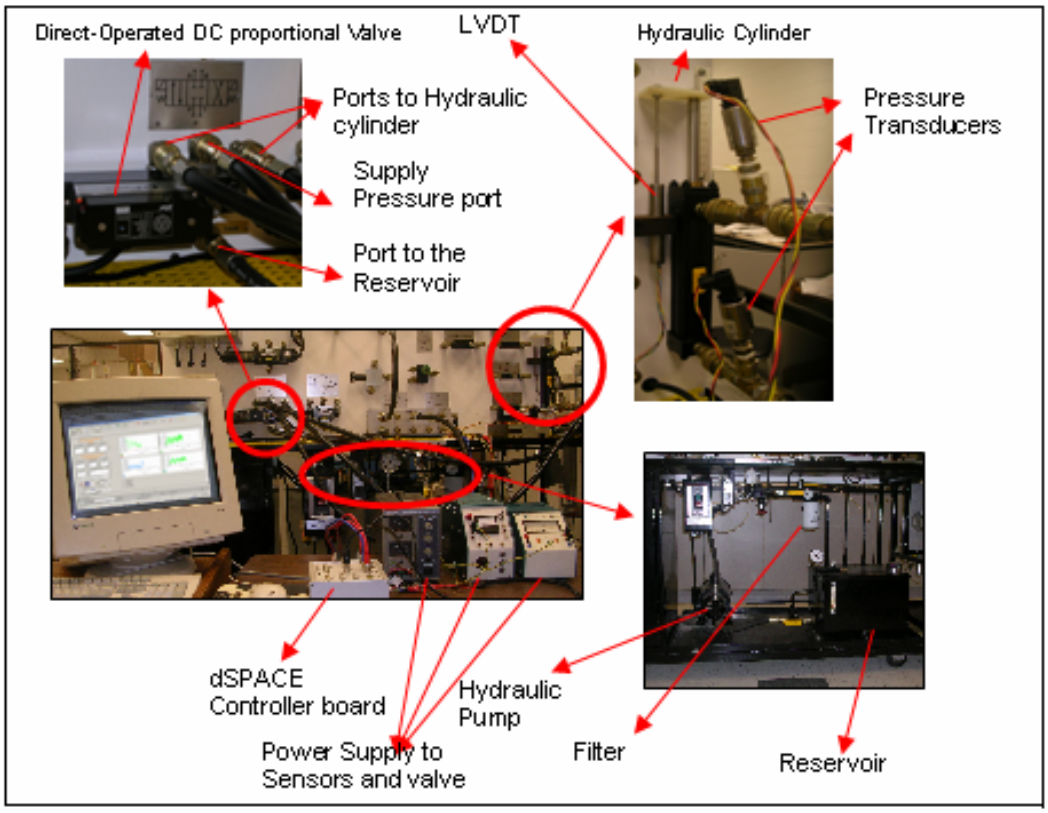

Figure C.1 Description of the hydraulic system